Homogenization and Wave Propagation Studies in Parametrically Modulated Structure and Honeycomb Composite

A Project Report

Submitted in partial fulfilment of the

requirements for the Degree of

Master of Engineering

in

Faculty of Engineering

by

Vijaykumar Chanda

Department of Aerospace Engineering

Indian Institute of Science

BANGALORE – 560 012

July 2008

TO

My parents

and

Sir

Acknowledgements

I would like to deeply express my gratitude to Prof. D.Roy Mahapatra for his constant and effective guidance in the current work. His presence along with timely insights was a great motivation in carrying forward this project with caution and interest. Working with him was a wonderful experience. His shrewd analysis and deep sense of subject helped me to understand things in the right perspective of research and its implications. I would also thank my colleagues Shiva shankar, Ashok, Anzar, Vivek, Pradeep and mithesh for synthesizing a congenial atmosphere in lab and are a source of constant support at difficult times. I would again express my deep gratitude to all my lab mates for their constant encouragement in my personal and professional life without which the project would not have been accomplished.

I would also thank my dear friends, Srinivas, Ramesha, Goutham, Krishna, Kiran and Shiva shankar for helping me especially in times of difficulty. I would like to acknowledge Prof. S. Gopala krishnana, Prof. Dinesh, Dr. S B. Kandagal for their valuable teaching of courses, these are very much helpful in my project work.

Vijay Kumar Chanda
Dept. of Aerospace Engg.
IISc.

Publications From This Project

1. "Wave Dispersion in A Cellular Composite with Modulated Microstructure",C. Vijay Kumar and D. Roy Mahapatra, *SPIE Proc. Behavior and Mechanics of Multifunctional and Composite Materials, Vol.6929, DOI:10.1117/12.776323, 2008*

2. *"Design of Cellular Composite Laminate for Vibration and Noise Control: Effects of Inclusions and Filling Patterns on the Acoustic Bandgaps",C. Vijay Kumar and D. Roy Mahapatra, Proceedings of ISSS 2008. (to appear) Int. conf. Smart Materials and Structures, July 24-27, 2008 Bangalore, India*

Abstract

A modeling technique and an analysis of wave dispersion in a cellular composite laminate with spatially modulated properties which can be modeled by parameterization and homogenization in an appropriate length scale are presented. By employing a higher order beam theory,the system of wave equations are derived. Homogenization of these equations are carried out in the scale of wavelength and frequency of individual wave modes. Dispersion relations for in-plane wave and flexural-shear wave are obtained. These dispersion relations are obtained for various values of stiffness modulation coefficients (α). For higher values of α ($\alpha = 6$) a repetitive stop band, pass band pattern is observed. For $\alpha = 0$ and $\alpha = 1$ group speeds are studied. Wave scattering at scales smaller than the order of cell size are filtered out in the present approach. To this end a beam is discretized by finite elements. Modulated material properties are employed and from the transverse velocity history, we observe the tendency to form stop bands for increasing values of stiffness modulation parameter, which is similar to the pattern observed from the wave dispersion analysis.

Next, the static homogenization and the dynamic homogenization of the honeycomb beam is presented. In the static homogenization, a unit-cell is chosen and its effective properties are obtained by using unintload method. Dynamic behavior of sandwich beam with honeycomb core structure is analyzed. The structure of the core is composed of a sequence of identical unit-cells repeating along the length and width of the beam. Each cell is composed of rectangular plate elements and assembled to form a three dimensional frame structure. Since each cell is filled with air, it will have an effect on the dynamic behavior of the beam. Therefore, the effect of cell wall pressure is considered in evaluating

the wavenumber. By using spectral finite element method, stiffness matrix for a unit-cell is formulated, and the global stiffness matrix of the honeycomb sandwhich beam is obtained by assembling the stiffness matrices. From the formulation frequency respnce of the sandwich beam under an external load is studied. It is observed from the frequency responce that, it is showing resonance behavior at some frequencies.

Contents

List of Tables

List of Figures

keywords

Cellular Composite, Wave Dispersion, Stiffness Modulation, Bandgap, Spectral element.

Chapter 1

Introduction

A cellular solid is one made up of an interconnected network of solid struts or plates which form the edges and faces of cells. The simplest form of cellular solid is a two-dimensional array of polygons which pack to fill a plane area like hexagonal cells of the bee; and for this reason we call such two-dimensional cellular materials honeycombs. More commonly, the cells are polyhedra which pack in three dimensions to fill space; we can such three-dimensional cellular materials foams. Almost any material can be foamed. Polymers, of course, are the most common. But metals, ceramics, glasses, and even composites, can be fabricated into cells. Three typical structures of cellular solids are shown in Fig. 1.2

Honeycomb sandwich materials are widely being used in weight sensitive and damping structures where high flexural rigidity is required, in many fields, especially, in the automobile industry. Honeycomb core sandwich panel is formed by adhering two high-rigidity thin-face sheets with a low-density honeycomb core possessing of low strength and stiffness. The vobrations of and the sound radiation from sandwich beams with truss core are analyzed by Ruzzene [1].

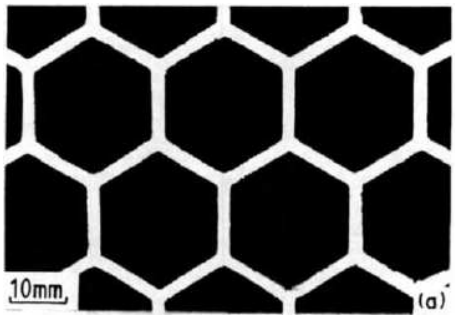

(a) a two dimensional honeycomb

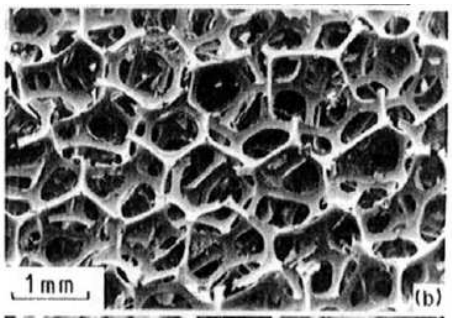

(b) a three dimensional foam with open cells

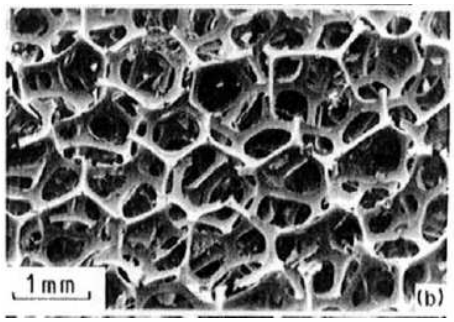

(c) a three dimensional foam with closed cells

Figure 1.1: Examples of cellular solids

1.1 Motivation

Sandwich panels made of honeycomb beams have found application in various areas such as aircraft structures, space vehicles, skis, racing yachts and portable buildings because of its attracting properties, light weight and more bending strength. With the help of honecomb sandwich panel, the vibration and noise can also be reduced.

Cellular composite materials with various types of microstructures [2] are potential candidates for applications in vibro-acoustic and aero-acoustic disturbance suppressions. The basic principle by which these composites enhance the disturbance suppression characteristics is the following. The cellular composites have microstructures, which deform very differently than the elastic continua. Due to the geometric features at multiple scales, the microstructure in a cellular composite shows certain resonance characteristics (often due to the highly flexible cell walls / ligaments). The resonance could originate either due to a single cell resonance or due to a network of cells behaving as coupled

resonator array. Incident disturbances with their characteristic power spectral densities (PSD) get transmitted through the cellular composite layers along the thickness direction and or in the laminate plane as a complicated function of frequency, wavelength and disturbance amplitude. This phenomenon leads to several challenges in designing the microstructures and other functionalities to suite a specific noise control application. The design approach could be based on the following aspects:

(1) Uniform microstructure (e.g., honeycomb type) with fixed resonance characteristics (optimal at a predefined and narrow frequency bands).

(2) Microstructure with randomly oriented ligaments (e.g., polymer foam). There exist several possibilities that a phenomenon of variable pressure air cavitation can be employed to alter the noise transmission characteristics over several frequency bands and hence to provide significant tunability.

(3) Uniform microstructure as backbone with polymer and bubble fillers (at smaller scales within the backbone cells). Various patterns of filled in cells and hollow cells in a honeycomb composite with face sheet, for example, can be realized for applications involving multiple tonal noise suppression.

1.2 Properties of Cellular solids

Foaming dramatically extends the range of properties availabel to the engineer. Cellular solids have physical, mechanical and thermal properties which are measured by the same methods as those used for fully dense solids. The density of cellular solid ranges typically ranges from 2 Kg/m^3 to $800Kg/m^3$ and that of true solids ranges from $900Kg/m^3$ 30,000 Kg/m^3 and youngs modulus of cellular solids ranges from $10^{-3}MN/m^2$ to $10^3MN/m^2$ where as for true solids it ranges from $10^3MN/m^3$ to $10^6MN/m^3$. These range properties of cellular solids in comparision with true solids is shown in Fig. **??**. This enormous extension of properties creates applications for foams which cannot be easily be filled by fully dense solids, and offers potential for engineering ingenuity. The low densities permit

the design of light, stiff components such as sandwich panels and large portable structures, and of flotation of all sorts. The low thermal conductivity allows cheap, reliable thermal insulation that can be bettered only by expensive vacuum-based methods. The low stiffness makes foams ideal for a wide range of cushioning applications; elastomeric foams, for instance, are the standard materials for seating. The low strengths and large compressive strains make foams attractive for energy-absorbing applications; there is an immense market for cellular solids for the protection of everything from computers to canisters of hazardous wastes.

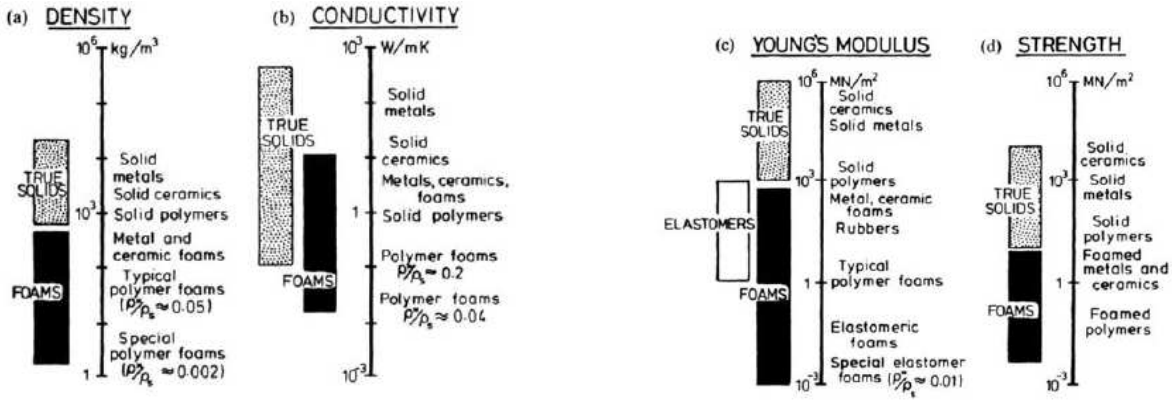

(a) density, thermal conductivity (b) Young's modulus, compressive strength

Figure 1.2: The range of properties available to the engineer through foaming

1.3 Applications of Cellular solids

There are majorly four areas of application of celluar materials: thermal insulation, packaging, structural use, and buoyancy. Besides this applications there are other smaller areas of application which are important, and growing. Thsese applications are in brief explained in this section.

1.3.1 Thermal insulation

The largest single application for polymeric and glass foams is as thermal insulation. Products as humble as disposable coffee cups, and as elaborate as the insulation of the

boster rockets for the space shuttle, exploit the low thermal conductivity.

1.3.2 Packaging

The second major use of man-made cellular solids is in packaging. An effective package mush absorb the energy of the system of impacts or of forces generated by deceleration without subjecting the contents to damaging stresses. Foams are particularly well suited for this.

1.3.3 Structural

Many natural structural materials are cellular solids: wood, cancellous bone, and coral all support large static and cyclic loads, for long periods of time. The structural use of natural cellular materials by man is as old as history itself. And increasingly, man-made foams and honeycombs are used in applications in which they perform a truly structural function. The most obvious example is their use in sandwich panels. Today, sandwich panels in modern aircraft use glass or carbon-fibre composite skins seperated by aluminium or paper-resin honeycombs, or by rigid polymer foams, giving a panel with enormous specific bending stiffness and strength. The same technology has spread to other applications where weight is critical: space vehicles, skis, racing yachts and portable buildings.

1.3.4 Buoyancy

Cellular materials found one of their earliest markets in marine buoyancy. Today, closed-cell plastic foams are extensively used as supports for floating structures and as floatation in boats.

1.4 Organization of the thesis

The thesis is organized in six chapters including this introduction.

- In Chapter 2, a review of literature on the recent advancements in the area of cellular solids and the objectives of the thesis are presented.
- Chapter 3 describes the mathematical formulation for wave propagation through microstructure and homogenization over wavelength scale, and harmonic wave approximation for the homogenized medium.
- Chapter 4 presents the longitudinal wave dispersion based on the mathematical model developed in Chapter 3 and focuses on investigating formation of stop bands. The transverse wave propagation in the composite laminate, associated dispersion relations and at the end validation of the proposed mathematical model using finite element method are also presented.
- In Chapter 5, static homogenization of the honeycomb beam is reported by using unit load method.
- Chapter 6 enumerates dynamic homogenization of the honeycomb sandwich beam by using spectral finite element method and inferences at the end
- Chapter 7 completes the thesis with the conclusions and future scope of the project.

Chapter 2

Literature Review

Published research and understanding on the subject of tunability of cellular composite are reviewed here first. The concept of tunable composite material is not new to the acoustics and wave mechanics research community. Mathematically, several models of wave propagation in such materials have been proposed. One approach of modeling is that of an effective homogenized medium through which elastic wave propagates, but the effective properties are assumed to be varying as a function of the spatio-temporal parameters. This is known as dynamic material [3]. With this approach, many researchers have reported wave dispersion behavior and transmission characteristics in rank-one type laminate (see e.g., ref. [4]). Analysis of wave propagation by assuming dynamic stiffness modulation has been reported by Sorokin and Grishina [5], which shows significant variation in the damping coefficients as a function of the stiffness modulation parameter, provided that such mechanisms can be realized in practice. Locally resonant band-gap phenomenon (as an extension to Helmholtz resonator cavities) have been analyzed by Wang and Ivansson [6], [7]. In ref. [6], the ratio of the attenuation constant and the phase constant and the frequency response function of the transmitted wave have been plotted over frequencies and certain band-gap was observed clearly. Damping of thin-walled honeycomb structures using energy absorbing foam was studied by Woody [8], which described the state of the art in vibration absorbing composite material technologies by using patterned fillers of passive polymer materials in honeycomb composite

with one face sheet. Similar research has been typically targeted to suppress the disturbance passively in space-based mirror. Related material system development, which is equally important for aero-acoustic and structure-born noise suppression is an open area of research.

It is only recently, that the features at the material microstructural scale (typically in millimeter scale and below) have been given due attention for passive-active application in vibration absorbing material system development. For example, an array of resonators attached to a one-dimensional structure and the resulting diffusive properties (useful for tunable damping) have been studied in [9].

2.1 Homogenization of Sandwich panel

The equivalent in-plane properties for hexagonal and re-entrant (auxetic) lattices are investigated through the analysis of partial differential equations associated with their homogenized continuum models by Stefano Gonella [11]. By taking the cell wall curvature into consideration the effective in-plane properties are are derived in [12]. The free flexural vibration of symmetric rectangular honeycomb panels is investigated by using the improved Reddys third-order theory in [13], but they have not introduced the effect of cell size.

2.2 conclusions and scope of the project

From the the review of literature, we have found that many researchers have done on sandwich panels, the effect of vibration and radiation through sandwich panel, also, some models to describe the dynamic behavior of sandwich panels. But, none of them considered the effect of cell size on the dispersion behavior of sandwich panel. And also, there is a need to find the dynamic behavior of honeycomb panel considering as three-dimensional frame structure. To this end the objectives of this project are described below.

- To develop a modeling technique for the cellular solids in order to determine the effect of stiffness modulation on the dispersion behavior in the cellular laminate, which will also introduce the effect of characteristic cell size.
- To determine the effective properties of the honeycomb beam under static loading.
- Dynamic homogenization of honeycomb sandwich beam, considering the honeycomb core of sandwich beam as a three dimensional frame.

Chapter 3

Mathematical formulation of governing equations of motion in a cellular beam

In order to determine the wave propagation characteristics, the cellular composite beam is modeled as a laminate with layer-wise parametrically modulated material properties. For better understanding of wave propagation we need to use a beam theory which can predict accurate interlaminar stress resultants. A Third-order shear deformation theory provides a parabolic distribution of the transverse shear stresses in the thickness direction and represents a close approximation to the true shear strain distribution for a plate and this can serve our purpose. This theory correctly accounts for traction-free condition on upper and lower surfaces of the beam while retaining the parabolic shear strain distribution across the beam thickness. Thereby eliminating the need for the use of shear correction factor.

Figure 3.1 shows a schematic diagram of general arrangement of cellular laminate. According to the third order beam theory, the kinematics in terms of the displacement field variable can be expressed as

$$u(x,z,t) = u^0(x,t) + z\phi(x,t) + z^2\bar{\phi}(x,t) + z^3\bar{\bar{\phi}}(x,t) \ ,$$

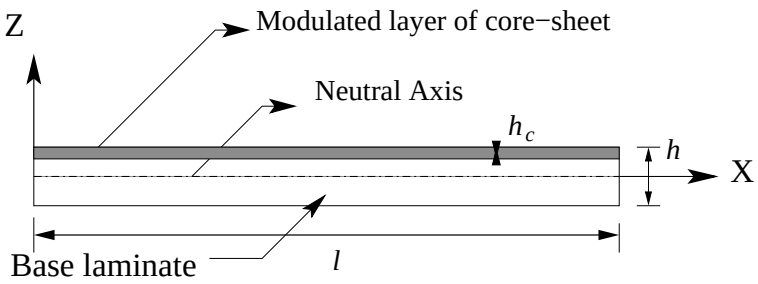

Figure 3.1: Schematic diagram of a layered composite with cellular microstructure which is modelled as parametrically modulated laminate.

$$w(x, z, t) = w^0(x, t). \tag{3.1}$$

where u is the total displacement parallel to X-axis, z denotes the depth coordinate measured with respect to the neutral axis, u^0 is the axial displacement along the neutral axis, w is the total displacement parallel to Z-axis, w^0 denotes the transverse displacement, ϕ is the slope of cross-sectional rotation measured at $z = 0$ and $\bar{\phi}$, $\bar{\bar{\phi}}$ are the higher-order distortions in the cross-section, which become significant for thick laminate (typically $l/h < 10$). Similarly, for the laminate with cellular microstructure (ref.Fig. 3.1), the displacement field beyond the resolution of the cell walls (t_w), $h_c >> t_w$, is modelled as

$$u_p(x, z, t) = u_p^0(x, t) + z\phi_p(x, t) + z^2\bar{\phi}_p(x, t) + z^3\bar{\bar{\phi}}_p(x, t) \ ,$$

$$w(x, z, t) = w_p^0(x, t). \tag{3.2}$$

where the subscript p denotes the cellular laminate. For a thin laminate under traction-free boundary conditions on top and bottom surfaces, the kinematics in Eq.(1) and Eq.(2) can be rewritten as

$$u(x, z, t) = u^0(x, t) + z\phi(x, t) + c_0 z^3 \left(\phi(x, t) + \frac{\partial w(x, t)}{\partial x} \right) ,$$

$$w(x, z, t) = w^0(x, t). \tag{3.3}$$

where $c_0 = -4/3h^2$, h is the overall thickness of the composite laminate. The strain

fields in the base laminate are expressed as

$$\epsilon_{xx} = \frac{\partial u}{\partial x} = \frac{\partial u^0}{\partial x} + z\frac{\partial \phi}{\partial x} + c_0 z^3 \left(\frac{\partial \phi}{\partial x} + \frac{\partial^2 w^0}{\partial x^2}\right) \ , \quad \epsilon_{yy} = \epsilon_{zz} = 0 \ , \tag{3.4}$$

$$\gamma_{xz} = \frac{\partial u}{\partial z} + \frac{\partial w}{\partial x} = \phi + 3c_0 z^2 \left(\phi + \frac{\partial w^0}{\partial x}\right) + \frac{\partial w^0}{\partial x} \ , \quad \gamma_{xy} = \gamma_{yz} = 0 \ . \tag{3.5}$$

For cellular laminate, the strain field becomes,

$$\epsilon_{xx_p} = \frac{\partial u_p}{\partial x} = \frac{\partial u_p^0}{\partial x} + z\frac{\partial \phi_p}{\partial x} + c_0 z^3 \left(\frac{\partial \phi_p}{\partial x} + \frac{\partial^2 w_p^0}{\partial x^2}\right) \ , \quad \epsilon_{yy_p} = \epsilon_{zz_p} = 0 \ ,$$

$$\gamma_{xz_p} = \frac{\partial u_p}{\partial z} + \frac{\partial w_p}{\partial x} = \phi_p + 3c_0 z^2 \left(\phi_p + \frac{\partial w_p^0}{\partial x}\right) + \frac{\partial w_p^0}{\partial x} \ ,$$

$$\gamma_{xy_p} = \gamma_{yz_p} = 0 \ . \tag{3.6}$$

with the above description of strain field, next we discuss constitutive modeling.

3.1 Constitutive modeling using parametric modulation

Let the characteristic length of each cell be λ_m in the cellular laminate. Let us also assume that the stiffness modulation is independent of time. The waves which are having wavelength smaller than the cell size are averaged. With the above assumptions the constitutive model is expressed as

$$\begin{Bmatrix} \sigma_{xx} \\ \tau_{xz} \end{Bmatrix} = \begin{bmatrix} \bar{Q}_{11} & 0 \\ 0 & \bar{Q}_{55} \end{bmatrix} \begin{Bmatrix} \epsilon_{xx} \\ \gamma_{xz} \end{Bmatrix} \ , \begin{Bmatrix} \sigma_{xx_p} \\ \tau_{xz_p} \end{Bmatrix} = \begin{bmatrix} \bar{Q}_{11_p} & 0 \\ 0 & \bar{Q}_{55_p} \end{bmatrix} \begin{Bmatrix} \epsilon_{xx_p} \\ \gamma_{xz_p} \end{Bmatrix} . \tag{3.7}$$

Cellular layer properties are given by

$$\bar{Q}_{11_p}(x,t) = \bar{Q}_{11}\left[1 + \alpha_1 \sin\left(\frac{2\pi x}{\lambda_m} + \theta\right)\right] , \tag{3.8}$$

$$\bar{Q}_{55_p}(x,t) = \bar{Q}_{55}\left[1 + \alpha_2 \sin\left(\frac{2\pi x}{\lambda_m} + \theta\right)\right], \tag{3.9}$$

$$\rho_p(x,t) = \rho\left[1 + \alpha_3 \sin\left(\frac{2\pi x}{\lambda_m} + \theta\right)\right]. \tag{3.10}$$

where $\bar{Q}_{11}$ is the longitudinal in-plane elastic modulus, $\bar{Q}_{55}$ is the shear modulus, ρ is the reference mass density, α_1, α_2 are the stiffness modulation parameters and α_3 is the density modulation parameter, λ_m is the characteristic cell dimension and θ is a phase angle between the incident wave and the corresponding mode of deformation in the cell walls. In order to simplify the homogenization problem at hand, we further assume α_1=α_2=α_3 in Eqs.(3.8)-(3.10).

The modulated stiffness and density in Eqs.(3.8)-(3.10) essentially approximates the stiffness and mass concentrated regions corresponding to the wall to wall connection periodically in the cellular laminate.

In order to derive the governing equations of motion with the above idealization, we apply Hamilton's first principal; that is,

$$\delta \int_{t_1}^{t_2} (\Gamma - U)\, dt = 0\ , \tag{3.11}$$

where $\delta(.)$ denotes the first variation, Γ and U are kinetic energy and the strain energy of the beam, respectively. These are given by

$$\Gamma = \int_0^l \int_A \left(\frac{1}{2}\rho\dot{u}^2 + \frac{1}{2}\rho\dot{w^0}^2\right) dAdx\ ,$$

$$U = \int_0^l \int_A \left(\frac{1}{2}\sigma_{xx}\epsilon_{xx} + \frac{1}{2}\tau_{xz}\gamma_{xz}\right) dAdx\ ,$$

where A is the area of cross section of the beam. Upon simplification using equations (3)-(5) and by applying calculus of variation, one obtains the governing equation of motion in the plane as

$$\delta u^0 :\ -\int_A \rho(x) dA\ddot{u}^0 - \int_A \rho(x) z dA\ddot{\phi} - \int_A \rho(x) c_0 z^3 dA\ddot{\phi} -$$

$$\int_A \rho(x) c_0 z^3 dA \frac{\partial \ddot{w}^0}{\partial x} + \int_A \frac{\partial \bar{Q}_{11}}{\partial x} dA \frac{\partial u^0}{\partial x} + \int_A \frac{\partial \bar{Q}_{11}}{\partial x} \left(z + c_0 z^3\right) dA \frac{\partial \phi}{\partial x} +$$
$$\int_A \frac{\partial \bar{Q}_{11}}{\partial x} c_0 z^3 dA \frac{\partial^2 w^0}{\partial x^2} + \int_A \bar{Q}_{11} dA \frac{\partial^2 u^0}{\partial x^2} + \int_A \bar{Q}_{11} \left(z + c_0 z^3\right) dA \frac{\partial^2 \phi}{\partial x^2}$$
$$+ \int_A \bar{Q}_{11} c_0 z^3 dA \frac{\partial^3 w^0}{\partial x^3} = 0. \tag{3.12}$$

For the cellular layer we substitute the form of parametric modulation from equations (8-10) and $\rho(x) = \rho_p(x)$ and $\bar{Q}_{11} = \bar{Q}_{11_p}$ in equation (12). The integrals due to thickness integration are given by

$$I_i = \int \rho z^i dz \ , i = 1, 2, ...6$$
$$A_{ii} = \int \bar{Q}_{ii} dz \ , \quad B_{ii} = \int \bar{Q}_{ii} z dz \ , \quad D_{ii} = \int \bar{Q}_{ii} z^2 dz \ , \quad F_{ii} = \int \bar{Q}_{ii} z^3 dz$$
$$f(\lambda_m, \theta) = \alpha_j \sin\left(\frac{2\pi x}{\lambda_m} + \theta\right) \ , \quad f' = \frac{\partial f}{\partial x} \ , \quad f'' = \frac{\partial^2 f}{\partial x^2}$$
$$H_{ii} = \int \bar{Q}_{ii} z^4 dz \ , \quad L_{ii} = \int \bar{Q}_{ii} z^6 dz \ , \tag{3.13}$$

Finally, we rewrite Eq. (12) using the above integral terms as

$$\delta u^0 : -I_0 \left[1 + f(\lambda_m, \theta)\right] \ddot{u}^0 - (I_1 + c_0 I_3) \left[1 + f(\lambda_m, \theta)\right] \ddot{\phi} -$$
$$c_0 I_3 \left[1 + f(\lambda_m, \theta)\right] \frac{\partial \ddot{w}}{\partial x} + A_{11} f'(\lambda_m, \theta) \frac{\partial u^0}{\partial x} + (B_{11} + c_0 F_{11}) f'(\lambda_m, \theta) \frac{\partial \phi}{\partial x} +$$
$$c_0 F_{11} f'(\lambda_m, \theta) \frac{\partial^2 w}{\partial x^2} + A_{11} \left[1 + f(\lambda_m, \theta)\right] \frac{\partial^2 u^0}{\partial x^2} + (B_{11} + c_0 F_{11})$$
$$\left[1 + f(\lambda_m, \theta)\right] \frac{\partial^2 \phi}{\partial x^2} + c_0 F_{11} \left[1 + f(\lambda_m, \theta)\right] \frac{\partial^3 w^0}{\partial x^3} = 0. \tag{3.14}$$

Note that this leads to a partial differential equations with spatially variable coefficients. Therefore these coefficients are needed to be homogenized over wavelength scale. This we will discuss in the next section. Similar to the in-plane equations, we obtain governing

equation for the flexural motion as

$$\delta w^0 : \int_A \frac{\partial}{\partial x}\left(\rho(x)\ddot{u}\right) c_0 z^3 - \int_A \left(\rho(x)\ddot{w^0}\right) - \int_A \frac{\partial^2}{\partial x^2}\left(\bar{Q}_{11}\epsilon_{xx}\right) c_0 z^3 +$$

$$\int_A \frac{\partial}{\partial x}\left(\bar{Q}_{11}\gamma_{xz}\right) 3c_0 z^2 + \int_A \frac{\partial}{\partial x}\left(\bar{Q}_{55}\gamma_{xz}\right) = 0 \ , \tag{3.15}$$

and after expansion, we get

$$\int_A \frac{\partial \rho(x)}{\partial x} c_0 z^3 dA \ddot{u^0} + \int_A \frac{\partial \rho(x)}{\partial x}\left(c_0 z^4 + c_0^2 z^6\right) dA \ddot{\phi} - \int_A \rho(x) dA \ddot{w^0}$$

$$+ \int_A \rho(x) c_0 z^3 dA \frac{\partial \ddot{u^0}}{\partial x} + \int_A \frac{\partial \rho(x)}{\partial x} c_0^2 z^6 dA \frac{\partial \ddot{w^0}}{\partial x} + \int_A \rho(x)\left(c_0 z^4 + c_0^2 z^6\right) dA \frac{\partial \ddot{\phi}}{\partial x}$$

$$+ \int_A \rho(x) c_0^2 z^6 dA \frac{\partial^2 \ddot{w^0}}{\partial x^2} + \int_A \frac{\partial \bar{Q}_{55}}{\partial x}\left(1 + 6c_0 z^2 + 9c_0^2 z^4\right) dA \phi$$

$$- \int_A \frac{\partial^2 \bar{Q}_{11}}{\partial x^2} c_0 z^3 dA \frac{\partial u^0}{\partial x} + \int_A \frac{\partial \bar{Q}_{55}}{\partial x}\left(1 + 6c_0 z^2 + 9c_0^2 z^4\right) dA \frac{\partial w^0}{\partial x} -$$

$$\int_A \left(\frac{\partial^2 \bar{Q}_{11}}{\partial x^2} c_0 z^4 - 6c_0 z^2 \bar{Q}_{55} - \bar{Q}_{55} + \frac{\partial^2 \bar{Q}_{11}}{\partial x^2} c_0^2 z^6 - \bar{Q}_{55} 9c_0^2 z^4\right) dA \frac{\partial \phi}{\partial x}$$

$$- \int_A \left(\bar{Q}_{55}\left(9c_0^2 z^4 + 3c_0 z^2 + 1 + 3c_0 z^2\right) + \frac{\partial^2 \bar{Q}_{11}}{\partial x^2} c_0^2 z^6\right) \frac{\partial^2 w^0}{\partial x^2} dA$$

$$-2 \int_A \frac{\partial \bar{Q}_{11}}{\partial x} c_0 z^3 dA \frac{\partial^2 u^0}{\partial x^2} + 2 \int_A \frac{\partial \bar{Q}_{11}}{\partial x}\left(2c_0 z^4 + 2c_0^2 z^6\right) dA \frac{\partial^2 \phi}{\partial x^2}$$

$$- \int_A \bar{Q}_{11} c_0 z^3 dA \frac{\partial^3 u^0}{\partial x^3} - 2 \int_A \frac{\partial \bar{Q}_{11}}{\partial x} c_0^2 z^6 dA \frac{\partial^3 w^0}{\partial x^3}$$

$$- \int_A \bar{Q}_{11}\left(c_0 z^4 + c_0^2 z^6\right) dA \frac{\partial^3 \phi}{\partial x^3} - \int_A \bar{Q}_{11} c_0^2 z^6 dA \frac{\partial^4 w^0}{\partial x^4} = 0. \tag{3.16}$$

With the help of the notations given in Eq. (13) for thickness integrated coefficients, the Eq. (16) can be rewritten as

$$c_0 I_3 f'(\lambda_m, \theta)\ddot{u^0} + \left(c_0 I_4 + c_0^2 I_6\right) f'(\lambda_m, \theta)\ddot{\phi} + c_0^2 I_6 f'(\lambda_m, \theta)\frac{\partial \ddot{w^0}}{\partial x}$$

$$+c_0 I_3[1+f(\lambda_m,\theta)]\frac{\partial \ddot{u}^0}{\partial x}+(c_0 I_4+c_0^2 I_6)[1+f(\lambda_m,\theta)]\frac{\partial \ddot{\phi}}{\partial x}+$$

$$c_0^2 I_6\left[1+f(\lambda_m,\theta)\right]\frac{\partial^2 \ddot{w}^0}{\partial x^2}-I_0\left[1+f(\lambda_m,\theta)\right]\ddot{w}^0$$

$$+\Big\{6c_0 D_{55}f'(\lambda_m,\theta)+A_{55}f'(\lambda_m,\theta)+9c_0^2 H_{55}f'(\lambda_m,\theta)\Big\}\phi$$

$$-c_0 F_{11}f''(\lambda_m,\theta)\frac{\partial u^0}{\partial x}+\Big\{9c_0^2 H_{55}f'(\lambda_m,\theta)+6c_0 D_{55}f'(\lambda_m,\theta)+A_{55}$$

$$f'(\lambda_m,\theta)\Big\}\frac{\partial w^0}{\partial x}+\Big\{\left(-c_0 H_{11}-c_0^2 L_{11}\right)f''(\lambda_m,\theta)+(6c_0 D_{55}+9c_0^2 H_{55}$$

$$+A_{55})[1+f(\lambda_m,\theta)]\Big\}\frac{\partial \phi}{\partial x}+\Big\{-c_0^2 L_{11}f''(\lambda_m,\theta)+(9c_0^2 H_{55}+6c_0 D_{55}$$

$$+A_{55})[1+f(\lambda_m,\theta)]\Big\}\frac{\partial^2 w^0}{\partial x^2}-\Big\{2c_0 F_{11}\frac{\partial^2 u^0}{\partial x^2}+(2c_0 H_{11}+2c_0^2 L_{11})\frac{\partial^2 \phi}{\partial x^2}$$

$$+2c_0^2 L_{11}\frac{\partial^3 w^0}{\partial x^3}\Big\}f'(\lambda_m,\theta)-c_0 F_{11}[1+f(\lambda_m,\theta)]\frac{\partial^3 u^0}{\partial x^3}$$

$$-(c_0 H_{11}+c_0^2 L_{11})[1+f(\lambda_m,\theta)]\frac{\partial^3 \phi}{\partial x^3}-c_0^2 L_{11}\frac{\partial^4 w^0}{\partial x^4}[1+f(\lambda_m,\theta)]\ . \tag{3.17}$$

Similarly, the equation of motion for cross sectional rotation ϕ is obtained as

$$\delta\phi:\ \int_A \rho(x)\ddot{u}z dA-\int_A \rho(x)z^2\ddot{u}c_0 z^3 dA+\int_A \frac{\partial}{\partial x}\left(\bar{Q}_{11}\epsilon_{xx}\right)z dA+$$

$$\int_A \frac{\partial}{\partial x}\left(\bar{Q}_{11}\epsilon_{xx}\right)c_0 z^3 dA-\int_A \bar{Q}_{55}\gamma_{xz}dA-\int_A \bar{Q}_{55}\gamma_{xz}3c_0 z^2 dA=0\ , \tag{3.18}$$

and after simplifying, it gives

$$\Big[-\left(I_1+c_0 I_3\right)\ddot{u}^0-\left(I_2+2c_0 I_4+c_0^2 I_6\right)\ddot{\phi}\Big]\left[1+f(\lambda_m,\theta)\right]$$

$$-\left(c_0 I_4+c_0^2 I_6\right)\left[1+f(\lambda_m,\theta)\right]\frac{\partial \ddot{w}^0}{\partial x}-\left(A_{55}+6c_0 D_{55}+9c_0^2 H_{55}\right)\left[1+f(\lambda_m,\theta)\right]\phi$$

$$+\left(B_{11}+c_0 F_{11}\right)\bar{f}'\frac{\partial u^0}{\partial x}-\left(6c_0 D_{55}+A_{55}+9c_0^2 H_{55}\right)\left[1+f(\lambda_m,\theta)\right]\frac{\partial w^0}{\partial x}$$

$$+\left(D_{11}+2c_0H_{11}+c_0^2L_{11}\right)\bar{f}'\frac{\partial\phi}{\partial x}+\left(B_{11}+c_0F_{11}\right)\left[1+f(\lambda_m,\theta)\right]\frac{\partial^2u^0}{\partial x^2}$$

$$+\left(c_0H_{11}+c_0^2L_{11}\right)\bar{f}'\frac{\partial^2w^0}{\partial x^2}+\left(D_{11}+2c_0H_{11}+c_0^2L_{11}\right)\left[1+f(\lambda_m,\theta)\right]\frac{\partial^2\phi}{\partial x^2}$$

$$+\left(c_0H_{11}+c_0^2L_{11}\right)\left[1+f(\lambda_m,\theta)\right]\frac{\partial^3w^0}{\partial x^3}=0\ . \tag{3.19}$$

Thus by using Hamilton's principle we obtained the governing equations of motion for in-plane, transverse and shear waves. All these equations (3.14), (3.17) and (3.19) are equations with spatially varying coefficient. The spatially varying parameters are f, f' and f'' as functions of space variable x. These quantities are homogenized in the wavelength scale.

3.2 Homogenization in wavelength scale

The functions f, f' and f'' are homogenized by integrating over half wave length ($\lambda/2$). The homogenized functions are indicated as $\bar{f}$, $\bar{f}'$ and $\bar{f}''$, respectively. We write

$$\bar{f}=\frac{2}{\lambda}\int_0^{\lambda/2}f(\lambda_m,\theta)dx\ .$$

Substituting for $f(\lambda_m,\theta)$ from Eq. (3.13), one has

$$\bar{f}=\frac{2}{\lambda}\int_0^{\lambda/2}\alpha_j\sin\left(\frac{2\pi x}{\lambda_m}+\theta\right)dx\ ,$$

and after simplification, we get

$$\bar{f}=\frac{\alpha_j}{\pi}\frac{\lambda_m}{\lambda}\left[-\cos\left(\frac{\pi}{\lambda_m/\lambda}+\theta\right)+\cos\theta\right]\ . \tag{3.20}$$

When $\lambda_m/\lambda=1$, the reduced form is

$$\bar{f}=\frac{\alpha_j}{\pi}2\cos\theta\ ,$$

and for $\lambda_m/\lambda >> 1$, $\bar{f} = 0$. In a similar way, homogenizing f' over $\lambda/2$, we get

$$\bar{f}' = \frac{2}{\lambda}\int_0^{\lambda/2} f'(\lambda_m,\theta)dx = \frac{2}{\lambda}\int_0^{\lambda/2} \frac{\partial}{\partial x}\left(\alpha_j \sin\frac{2\pi x}{\lambda_m} + \theta\right) dx \ ,$$

$$\Rightarrow \bar{f}' = \frac{2}{\lambda}\alpha_j \left[\sin\left(\frac{\pi\lambda}{\lambda_m} + \theta\right) - \sin\theta\right] . \tag{3.21}$$

When $\lambda_m/\lambda = 1$,

$$\bar{f}' = -\frac{4}{\lambda}\alpha_j \sin\theta \ ,$$

and when $\lambda_m/\lambda >> 1$, $\bar{f}' \approx 0$. $\lambda_m/\lambda = 1$ is the case when cell characteristic length is equal to incident wavelength and $\lambda_m/\lambda = 1$ is the case when characteristic length of the cell is very much higher than the incident wave length. Next, homogenizing $\bar{f}''$ over $\lambda/2$, we get

$$\bar{f}'' = \frac{2}{\lambda}\int_0^{\lambda/2} f''(\lambda_m,\theta)dx = \bar{f}'' = \frac{4\pi\alpha_j}{\lambda\lambda_m}\left[-\sin\left(\frac{\pi}{\lambda_m/\lambda} + \theta\right) + \sin\theta\right] . \tag{3.22}$$

When $\lambda_m/\lambda = 1$, one has

$$\bar{f}'' = \frac{8\pi\alpha_j}{\lambda_m^2}\sin\theta \ ,$$

and when $\lambda_m/\lambda >> 1$, $\bar{f}'' = 0$. With the homogenized quantities above, we analyze the dispersion characteristics in the next section.

3.3 Harmonic wave approximation for the homogenized medium

Here we consider multimode harmonic wave approximation for the field variables u^0, w and ϕ of following form

$$u^0(x,t) = \sum_n \tilde{u}(\omega_n)e^{i(\omega_n t - kx)} \ , \quad w^0(x,t) = \sum_n \tilde{w}(\omega_n)e^{i(\omega_n t - kx)} \ ,$$

$$\phi = \sum_n \tilde{\phi}(\omega_n) e^{i(\omega_n t - kx)} \ . \tag{3.23}$$

where $\omega = \omega_n$ is the sampling frequency, $k(\omega)$ is the wave number and $(\tilde{.})$ denotes the wave amplitude. Substituting the harmonic waveform in governing equation of motion in inplane given in Eq. (3.14) and using the homogenized quantities defined in section. 3.2, we get

$$m_{11}\tilde{u} + m_{12}\tilde{w} + m_{13}\tilde{\phi} = 0 \ , \tag{3.24}$$

where

$$m_{11} = I_0(1+\bar{f})\omega^2 - iA_{11}\bar{f}'k - A_{11}(1+\bar{f})k^2 \ ,$$

$$m_{12} = -ic_0 I_3(1+\bar{f})\omega^2 k - c_0 F_{11}\bar{f}'k^2 + ic_0 F_{11}(1+\bar{f})k^3 \ ,$$

$$m_{13} = (I_1 + c_0 I_3)\,(1+\bar{f})\omega^2 - i\left(B_{11}\bar{f}' + c_0 F_{11}\bar{f}'\right)k - \left(B_{11} + c_0 F_{11}\right)(1+\bar{f})k^2 \ .$$

Similarly, the governing equation for flexural motion given in Eq. (3.17) is reduced to

$$m_{21}\tilde{u} + m_{22}\tilde{w} + m_{23}\tilde{\phi} = 0 \ , \tag{3.25}$$

where

$$m_{21} = -c_0 I_3 \bar{f}'\omega^2 + i\left(c_0 I_3(1+\bar{f})\omega^2 + c_0 F_{11}\bar{f}''\right)k + 2c_0 F_{11}\bar{f}'k^2$$

$$-ic_0 F_{11}(1+\bar{f})k^3 \ ,$$

$$m_{22} = I_0(1+\bar{f})\omega^2 + i\left(c_0^2 I_6\omega^2 - 9c_0^2 H_{55} - 6c_0 D_{55} - A_{55}\right)\bar{f}'k +$$

$$\Big(c_0^2 L_{11}\bar{f}'' - \left(c_0^2 I_6\omega^2 + 9c_0^2 H_{55} + 6c_0 D_{55} + A_{55}\right)(1+\bar{f})\Big)k^2 - 2ic_0^2 L_{11}\bar{f}'k^3$$

$$-c_0^2 L_{11}(1+\bar{f})k^4 \ ,$$

$$m_{23} = \left(6c_0 D_{55} + 9c_0^2 H_{55} + A_{55}\right)\bar{f}' - \left(c_0 I_4 + c_0^2 I_6\right)\bar{f}'\omega^2 + i\Big(c_0 H_{11}\bar{f}'' +$$

$$c_0^2 L_{11}\bar{f}'' - \left(-c_0^2 I_6\omega^2 - c_0 I_4\omega^2 + 6c_0 D_{55} + 9c_0^2 H_{55} + A_{55}\right)(1+\bar{f})\Big)k$$

$$+\left(2c_0 H_{11} + 2c_0^2 L_{11}\right)\bar{f}'k^2 - i\left(c_0 H_{11} + c_0^2 L_{11}\right)(1+\bar{f})k^3 \ .$$

Similarly, the governing equation of motion for cross sectional rotation given in Eq. (3.19) is reduced to

$$m_{31}\tilde{u} + m_{32}\tilde{w} + m_{33}\tilde{\phi} = 0 \ , \tag{3.26}$$

where

$$m_{31} = (I_1 + c_0 I_3)\,(1+\bar{f})\omega^2 - i\,(B_{11} + c_0 I_{11})\,\bar{f}'k - (B_{11} + c_0 F_{11})\,(1+\bar{f})k^2 \ ,$$

$$m_{32} = -i\left(\left(c_0 I_4 + c_0^2 I_6\right)\omega^2 k - (6c_0 D_{55} + A_{55} + 9c_0^2 H_{55})\right)(1+\bar{f})k$$

$$-\left(c_0 H_{11} + c_0^2 L_{11}\right)\bar{f}'k^2 + i\left(c_0 H_{11} + c_0^2 L_{11}\right)(1+\bar{f})k^3 \ ,$$

$$m_{33} = \left(I_2 + 2c_0 I_4 + c_0^2 I_6\right)(1+\bar{f})\omega^2 - i\left(D_{11} + 2c_0 H_{11} + c_0^2 L_{11}\right)\bar{f}'k$$

$$-\left(D_{11} + 2c_0 H_{11} + c_0^2 L_{11}\right)(1+\bar{f})k^2 - \left(A_{55} + 6c_0 D_{55} + 9c_0^2 H_{55}\right)(1+\bar{f}) \ .$$

Rewriting equations (26)-(28) in matrix form as

$$\Big[m(\omega, \alpha, \lambda_m, \theta, k(\omega))\Big]\begin{Bmatrix}\tilde{u}\\ \tilde{w}\\ \tilde{\phi}\end{Bmatrix} = \begin{Bmatrix}0\\ 0\\ 0\end{Bmatrix} \ , \tag{3.27}$$

we get the dispersion equation as Det[m]=0, which needs to be solved in (ω, k) space. Our objective is to understand this $k-w_n$ curves as a function of the material parameters (α, λ_m, θ).

The dispersion analysis of cellular composite laminate is carried out in the next section.

Chapter 4

Analysis of Wave Dispersion in A Parametrically Modulated Laminate

With the help of the governing equations derived in the previous chapter and homogenized quantities, dispersion analysis is presented in this chapter. First longitudinal or in-plane wave dispersion is analyzed and then wave dispersion relations for flexural-shear coupled case is analyzed.

4.1 Longitudinal wave dispersion

For longitudinal wave propagation alone, we omit the flexural terms and with reference to Eq. (3.27), we set

$$m_{11} = 0$$

$$\Rightarrow I_0(1+\bar{f})\omega^2 - iA_{11}\bar{f}'k - A_{11}(1+\bar{f})k^2 = 0\ .$$

By solving this quadratic equation for k, one has

$$k = -\frac{i}{2}\frac{\bar{f}'}{(1+\bar{f})} \pm \sqrt{\frac{I_0\omega^2}{A_{11}} - \left(\frac{\bar{f}'}{2(1+\bar{f})}\right)^2}\ . \tag{4.1}$$

The longitudinal wave will not propagate if k is imaginary. For this to happen, the descriminent in the above equation should be negative or zero; that is when

$$\left|\frac{\bar{f}'}{2(\bar{f}+1)}\right| \geq \omega\sqrt{\frac{I_0}{A_{11}}}\,. \tag{4.2}$$

By substituting the expressions for $\bar{f}$ and $\bar{f}'$ from Eqs. (3.20) and (3.21) respectively, Eq. (4.2) is rewritten as

$$\left|\frac{\frac{2}{\lambda}\alpha\left[\sin\left(\pi\frac{\lambda}{\lambda_m}+\theta\right)-\sin\theta\right]}{2\left[1+(\frac{\alpha}{\pi})\frac{\lambda_m}{\lambda}\left\{\cos\theta-\cos\left(\theta+\pi\frac{\lambda}{\lambda_m}\right)\right\}\right]}\right| \geq \omega\sqrt{\frac{I_0}{A_{11}}}$$

$$\Rightarrow \omega \leq \sqrt{\frac{A_{11}}{I_0}}\left|\frac{\frac{2\alpha}{\lambda}\left[\sin\left(\pi\frac{\lambda}{\lambda_m}+\theta\right)-\sin\theta\right]}{2\left[1+\left(\frac{\alpha}{\pi}\right)\left(\frac{\lambda_m}{\lambda}\right)\left\{\cos\theta-\cos\left(\theta+\pi\frac{\lambda}{\lambda_m}\right)\right\}\right]}\right|\,. \tag{4.3}$$

Therefore, for all the frequencies that satisfy the above relation, the in-plane wave will not propagate. The frequency band over which there is no wave propagation (Re[k]=0) is called a stop band. And the frequency band over which the wave propagates ($Re[k] \neq 0$) is called a pass band. We consider a configuration as shown in Fig. 4.1, in this configuration the cellular solid is a part of a rigid baffle of infinite length. Hence a wave generated in the rigid baffle is the incident wave for the cellular beam. The wavelength in the rigid baffle is evaluated by considering it as a bar made of Aluminum. The wavelength (λ) is evaluated as

$$\lambda = \frac{2\pi}{\omega}\sqrt{\frac{Q}{\rho}}\,, \tag{4.4}$$

here by taking $Q = Q_{11}$ we get the wavelength of a flexural wave coming into the cellular

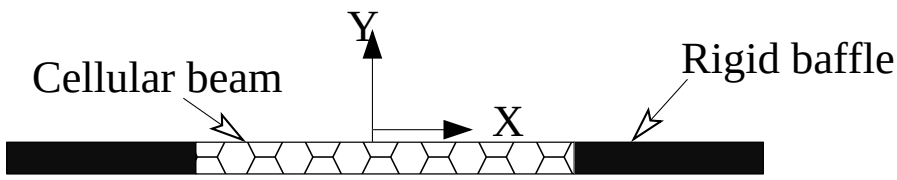

Figure 4.1: Cellular laminated beam placed between two baffles

laminate, similarly by taking $Q = Q_{55}$ we get the wavelength of a shear wave coming into

the cellular laminate. The right hand side of the Eq. (4.3) can be defined as a critical frequency, because this limits the propagation of the wave. Therefore a critical frequency (ω_c) is defined as

$$\omega_c = \sqrt{\frac{A_{11}}{I_0}} \left| \frac{\frac{2\alpha}{\lambda}\left[\sin\left(\pi\frac{\lambda}{\lambda_m}+\theta\right)-\sin\theta\right]}{2\left[1+\left(\frac{\alpha}{\pi}\right)\left(\frac{\lambda_m}{\lambda}\right)\left\{\cos\theta-\cos\left(\theta+\pi\frac{\lambda}{\lambda_m}\right)\right\}\right]} \right| . \tag{4.5}$$

For an applied frequency ω, when $\omega_c \geq \omega$, there will be no propagation, that is when $\omega_c/\omega \geq 1$ the corresponding band of frequencies is called a stop-band. When $\omega_c/\omega < 1$, there will be propagation of wave, and hence it is called as pass band.

We consider an Aluminum beam with a cross section $30\,mm \times 30\,mm$ and length $60\,cm$. Following material properties are used for the considered beam. $Q_{11} = 70 \times 10^9\,N/m^2$, $\rho = 2600\,Kg/m^3$ and $\nu = 0.33$, these are of common Aluminum material properties. Here Q_{55} is calculated from the relation $Q_{55} = Q_{11}/(2(1+\nu))$. The characteristic length λ_m is taken as $8\,mm$.

In the Eq. (4.5) the critical frequency (ω_c) is evaluated by taking the incident wave phase angle $\theta = 60^o$. For various values of α, $\alpha = 0,\ 2,\ 4,\ 6$ in the Eq. (4.5) ω_c is evaluated. Fig. 4.2 shows ω_c/ω vs λ_m/λ for various values of α.

From the Eqs. (3.20) and (3.21), when $\alpha = 0$, $\bar{f} = 0$ and $\bar{f}' = 0$. Therefore from Eq. (4.1) the wave number k becomes a real number. This means for $\alpha = 0$ the longitudinal wave will propagate in all frequency bands. The same charactestic is shown in the Fig. 4.2(a) for $\alpha = 0$.

From the figure 4.2(a) it is observed that, $\omega_c/\omega = 0$ for $\alpha = 0$ and for all values of λ_m/λ. This means the longitudinal wave will propagate through the beam for any value of λ. In the Fig. 4.2(a)-4.2(d) there is a line called reference line, shown in dotted line, if the ω_c/ω crosses this line there will be no progation. By studying figures 4.2(b)-4.2(d) we can observe that, as the stiffness modulation factor (α) increases, the value of ω_c/ω also moves towards the reference line ($\omega_c/\omega = 1$). From the Figs. 4.2(c)-4.2(d) the values of ω_c/ω cross the reference line intermitant frequency bands. Therefore in these frequency bands the wave do not propage, and these frequency bands are called stop bands. At

higher values of α for example $\alpha = 4\ ,6$ the pattern is that of a repetitive stop and pass bands. Next we consider the flexural-shear case and we analyze the dispersion relations to bring a conclusion on the effect of stiffness modulation (α).

4.2 Flexural-Shear wave dispersion

In order to obtain the transverse wave dispersion relation, we omit the terms corresponding to in-plane wave (first row and first column) in Eq. 3.27 we get a 2×2 system given by

$$\begin{bmatrix} m_{22} & m_{23} \\ m_{32} & m_{33} \end{bmatrix} \begin{Bmatrix} \tilde{w} \\ \tilde{\phi} \end{Bmatrix} = \begin{Bmatrix} 0 \\ 0 \end{Bmatrix} \tag{4.6}$$

The determinant of the above 2×2 matrix is the characteristic equation for flexural wave propagation; that is,

$$m_{22}m_{33} - m_{32}m_{23} = 0\ . \tag{4.7}$$

With the help of Eqs. (3.24)-(3.25) the expressions for m_{22}, m_{23}, m_{32} and m_{33} can be rewritten as polynomials of wave number (k) as

$$m_{22} = a_4k^4 + a_3k^3 + a_2k^2 + a_1k + a_0\ ,$$

$$m_{23} = b_3k^3 + b_2k^2 + b_1k + b_0\ ,$$

$$m_{32} = c_3k^3 + c_2k^2 + c_1k\ ,$$

$$m_{33} = d_2k^2 + d_1k + d_0\ ,$$

where

$$a_4 = -c_0^2L_{11}(1+\bar{f})\ , \quad a_3 = -2c_0^2L_{11}\bar{f}'\ ,$$

$$a_2 = c_0^2L_{11}\bar{f}'' - \left(c_0^2I_6\omega^2 + 9c_0^2H_{55} + 6c_0D_{55} + A_{55}\right)(1+\bar{f})\ ,$$

$$a_1 = i(c_0^2I_6\omega^2 - 9c_0^2H_{55} - 6c_0D_{55} - A_{55})\bar{f}'\ ,$$

$$a_0 = I_0(1+\bar{f})\omega^2 \ , \quad b_3 = -i(c_0 H_{11} + c_0^2 L_{11})(1+\bar{f}) \ ,$$

$$b_2 = (2c_0 H_{11} + 2c_0^2 L_{11})\bar{f}' \ ,$$

$$b_1 = -\left(-c_0^2 I_6 \omega^2 - c_0 I_4 \omega^2 + 6c_0 D_{55} + 9c_0^2 H_{55} + A_{55}\right)(1+\bar{f}) +$$

$$\left(c_0 H_{11} + c_0^2 L_{11}\right)\bar{f}'' \ ,$$

$$b_0 = \left(6c_0 D_{55} + 9c_0^2 + A_{55}\right)\bar{f}' \ , \quad c_3 = i(c_0 H_{11} + c_0^2 L_{11})(1+\bar{f}),$$

$$c_2 = -(c_0 H_{11} + c_0^2 L_{11})\bar{f}' \ ,$$

$$c_1 = -i\left(\left(c_0 I_4 + c_0^2 I_6\right)\omega^2 - \left(6c_0 D_{55} + A_{55} + 9c_0^2 H_{55}\right)\right)(1+\bar{f}) \ ,$$

$$d_2 = -(D_{11} + 2c_0 H_{11} + c_0^2 L_{11})(1+\bar{f}) \ ,$$

$$d_1 = -i(D_{11} + 2c_0 H_{11} + c_0^2 L_{11})\bar{f}' \ ,$$

$$d_0 = \left((I_2 + 2c_0 I_4 + c_0^2 I_6)\omega^2 - \left(A_{55} + 6c_0 D_{55} + 9c_0^2 H_{55}\right)\right)(1+\bar{f}) \ .$$

With the help of the above notations, the determinant in Eq. (4.7) is evaluated as

$$(a_4 k^4 + a_3 k^3 + a_2 k^2 + a_1 k + a_0)(d_2 k^2 + d_1 k + d_0) -$$

$$(b_3 k^3 b_2 k^2 + b_1 k + b_0)(c_3 k^3 + c_2 k^2 + c_1 k) = 0 \ , \tag{4.8}$$

which can be expressed in polynomial of wavenumber k as

$$X_6 k^6 + X_5 k^5 + X_4 k^4 + X_3 k^3 + X_2 k^2 + X_1 k + X_0 = 0 \ , \tag{4.9}$$

where

$$X_6 = a_4 d_2 - b_3 c_3, \ X_5 = a_4 d_1 + a_3 d_2 - b_3 c_2 - b_2 c_3 \ ,$$

$$X_4 = a_4 d_0 + a_3 d_1 + a_2 d_2 - b_3 c_1 - b_2 c_2 - b_1 c_3 \ ,$$

$$X_3 = a_3 d_0 + a_2 d_1 + a_1 d_2 - b_2 c_1 - b_1 c_2 - b_0 c_3 \ ,$$

$$X_2 = a_2 d_0 + a_1 d_1 + a_0 d_2 - b_1 c_1 - b_0 c_2 \ , \quad X_1 = a_1 d_0 + a_0 d_1 - b_0 c_1 \ ,$$

$$X_0 = a_0 d_0 \ .$$

There will be no wave propagation through the laminate when Re[k]=0. In addition to this when Im[k]$\neq$ 0, the system behaves as dissipative system. Further more, when Im[k]=0, the entire system will behave like a rigid body. By setting $k = 0$ in Eq. (4.9), we get

$$X_0 = a_0 d_0 = 0 \ .$$

This is true if $a_0 = 0$ or $d_0 = 0$ or both. Setting $a_0 = 0$, we get $\omega = 0$ which is essential in the static case and hence of not much use. Next by setting $d_0 = 0$ we get

$$\omega = \sqrt{\frac{(A_{55} + 6c_0 D_{55} + 9c_0^2 H_{55})}{(I_2 + 2c_0 I_4 + c_0^2 I_6)}} \ , \tag{4.10}$$

which is always real. For the chosen material and geometry of the beam, we have $\omega = 14.49KHz$. This is a frequency at which, ideally the system will behave like a rigid body. However, since it will not localize any energy within it at this frequency, therefore for absorption of incident wave this will not serve the purpose of wave suppression.

By solving the full characteristic Eq. (4.9) we get dispersion curves. The dispersion curves for various stiffness modulation coefficients such as $\alpha = 0,\ 1,\ 3,\ 6$ are generated. The disperion curves with $Q = Q_{11}$ in Eq. (4.4) for various values of α are shown in Fig. 4.3.

From the Fig. 4.3(a) one can observe that, for $\alpha = 0$ the shear wave do not propagete upto a cut-off frequency ($\omega_{cutoff} = 52.52KHz$) and after cut-off frequency the shear wave will propagate, flexural wave propagates over completer frequency range. In the figure flexural wave is marked with k_1 and shear wave is marked with k_2. As the stiffness modulation factor (α) increases (see Figs. 4.3(b)-4.3(d)) shear wave and the flexural waves show a tendency to form repetitive stop bands. For $\alpha = 3$ in the Fig. 4.3(c) the shear wave forms repetitive stop bands, which is indicated by an arrow A. And the flexural wave also has a tendency to form stop bands, which is shown with an arrow B. For $\alpha = 6$, Fig. 3(d) shows that the shear wave forms many stop bands (shown with an

arrow A) and the absolute of real part of wavenumber (k_2) is decreasing althoughis it does not form stop bands completely for bands shown with an arrow B. For even higher values of α, the flexural wave also forms stop bands. Another observation one can make is that the clearly visible cut-off frequency (ω_c) seen in Fig. (4.3)(a) moves to effectively higher value (although not clearly identifiable) for higher values of α.

The disperion relations with $Q = Q_{55}$ in the Eq. (4.4) for various values of α are presented in the Fig. 4.4. From this figure one can observe a very similar behavior as in the previous case $Q = Q_{11}$. But in this case both the flexural and the shear waves are forms stop bands and pass bands even at lower values of α, particularly in Fig. (4.4)(d) for $\alpha = 6$. The formation of stop bands is indicates with arrow A in the figures 4.4(b)-(d) and flexural wave is indicated with an arrow B. The cut-off frequency is also increases as the α is increases.

The dispersion curves for $\lambda = \lambda_m$ are given in the Fig. 4.5. $\lambda = \lambda_m$ means when the wave-length of the incident wave (λ) is equal to the cell size (λ_m). In this case also an incident wave phase angle of $\theta = 60^o$ is used. We can see from the figure that as α increases from 0 to 1 both the shear and the flexural waves becomes almost completely evanescent in the Fig. 4.5(d). Although not modelled physically, because of cell wall resonance through the parametric representation of the material propertis.

Next, the group speeds and phase speeds of the beam are calculated for $\alpha = 0$ and $\alpha = 1$ from the characteristic equation (4.9). The phase speed is expressed as $c_p = \omega/k$ and the group speed is expressed as $c_g = d\omega/dk$. From the dispersion relations given in Fig. 4.3 the wave phase speeds are obtained directly. The phase speeds for $\alpha = 0$ and $\alpha = 1$ are given in Fig. 4.6. In this figure the phase speeds for $\alpha = 0$ is indicated by C_{p_0} and for $\alpha = 1$ it is indicated by C_{p_1}. Phase speed of the shear waves is indicated with an ellipse marked with B and the phase speed of the flexural wave is marked with A.

By differentiating the characteristic equation (Eq. (4.9)) with respect to ω and rearranging, we get,

$$\frac{dk}{d\omega} = -\frac{k^6\frac{dX_6}{d\omega} + k^5\frac{dX_5}{d\omega} + k^4\frac{dX_4}{d\omega} + k^3\frac{dX_3}{d\omega} + k^2\frac{dX_2}{d\omega} + k\frac{dX_1}{d\omega} + \frac{dX_0}{d\omega}}{6X_6k^5 + 5X_5k^4 + 4X_4k^3 + 3X_3k^2 + 2X_2k + X_1} .$$

In the above equation X_6 and X_5 are not a function of ω therefore we obtain the group speed as

$$C_g = Re\left[-\frac{6X_6k^5 + 5X_5k^4 + 4X_4k^3 + 3X_3k^2 + 2X_2k + X_1}{k^4\frac{dX_4}{d\omega} + k^3\frac{dX_3}{d\omega} + k^2\frac{dX_2}{d\omega} + k\frac{dX_1}{d\omega} + \frac{dX_0}{d\omega}}\right] . \tag{4.11}$$

By using above relation the dispersion of group speeds are generated for $\alpha = 0$ and $\alpha = 1$, which are shown in Fig. 4.7. In this figure, the group speeds for flexural wave are indicated with an ellipse marked with A and group speeds for shear wave are indicated with an ellipse marked with B. From the figure one can observe that for $\alpha = 1$ the shear wave group speed is a rapidly oscillating function of frequency. Therefore we can conclude that there is a tendency to form repetitive stop bands and pass bands as the stiffness modulation factor (α) increases.

4.3 Verification of Homogenization Results

Verification of the homogenization method used in this mathematical model is carried out by using finite element simulation. COMSOL Multiphysics package has been used for this purpose. For comparing the dispersion results consider a beam with the same geometry ($30\,mm \times 30\,mm$ cross section and $60\,cm$ length) as considered previously. A schematic drawing is shown in Fig. 4.3, it is fixed at one end (x=0) and a modulated pulse F of $100\,kHz$ is applied at the tip (x=L) of the beam. Elastic modulus (E) and density (ρ) are taken from Eqs. (3.8)-(3.10). The beam is descritized into 1328 triangular elements. A time dependent analysis is carried out. GMRES solver is used to solve the lenear system. A time step of 1.5×10^{-7} Sec is used. Velocity history is obtained at a point ($x = 10\,cm$), which is shown in the Fig. 4.3.

Velocity histories are obtained for stiffness modulation $\alpha = 0$ and $\alpha = 1$. As discussed earlier, that for $\alpha > 1$, the density becomes negative and also elastic constant becomes negative. However, in a sense of parametric representation the wave properties remain unaltered mathematically. With the standard finite element package, however there is

numerical problem while dealing with negative sign of the mass and stiffness matrix, especially when time integration method is adopted. Because of this reason, we restrict the numerical simulation to $\alpha \leq 1$. The velocity histories for $\alpha = 0$ and $\alpha = 1$ are shown in the Fig. (4.9).

The time for the wave to travel from point x=L=60 cm to x=l=10cm is estimated from the Fig. 4.9. The distance of travel is 50 cm. By using the traveling distance and traveling time the group speeds are evaluated. These group speeds are approximately equal to the group speeds correspondings to frequency 100 KHz evaluated using homogenization. The shear and flexural wave packets are identified with the help of the group speeds calculations and comparing with the group speeds from analytical method figure 4.7.

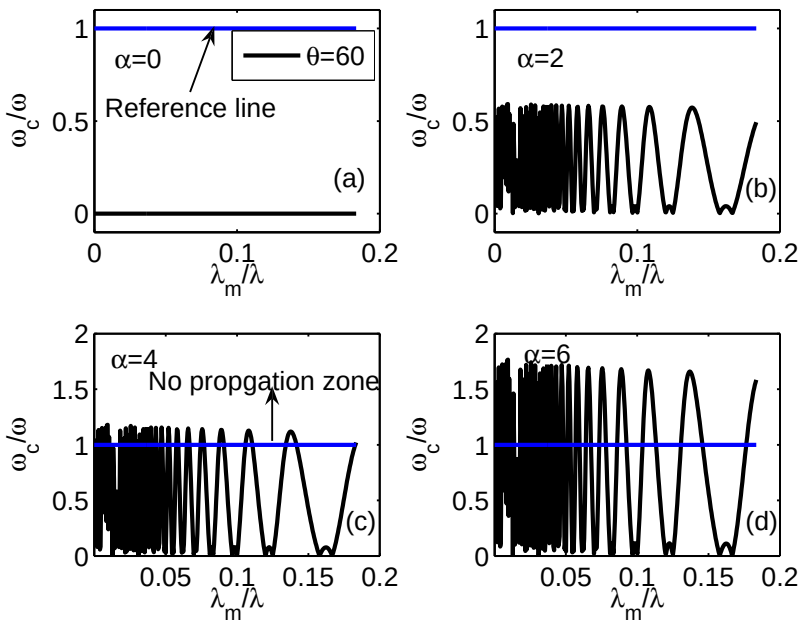

Figure 4.2: Stop band frequencies ($\omega_c/\omega \geq 1$ regions) computed for various incident waves. θ is the phase angle of the incident wave, $\theta = 60^o$ is used for all sub figures.

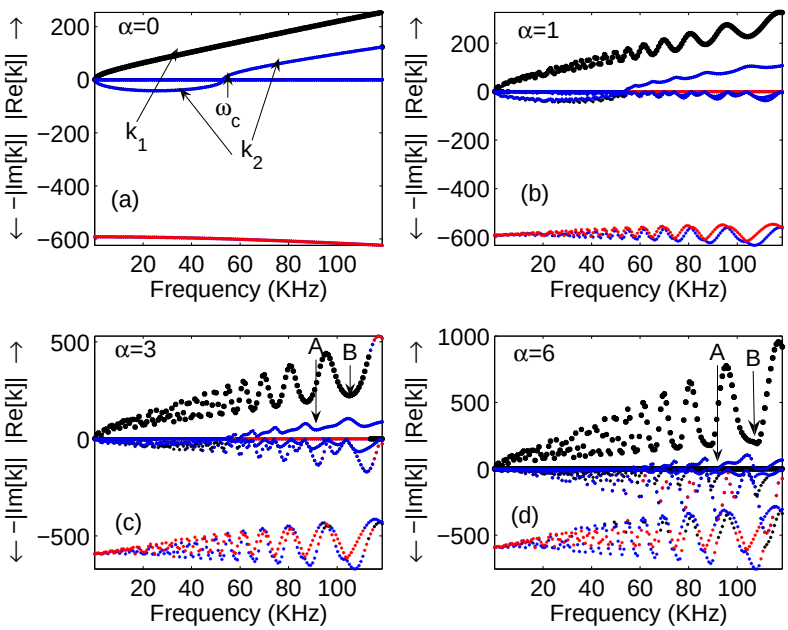

Figure 4.3: Dispersion behavior for various λ_m/λ when Q_{11} is used for evaluating the wavelength (λ) (see Eq. (4.4)), showing a tendency toward formation of stop bands for flexural and shear waves at higher frequencies (marked with arrows A and B), k_1 indicates flexural wave number and k_2 indicates shear wave number.

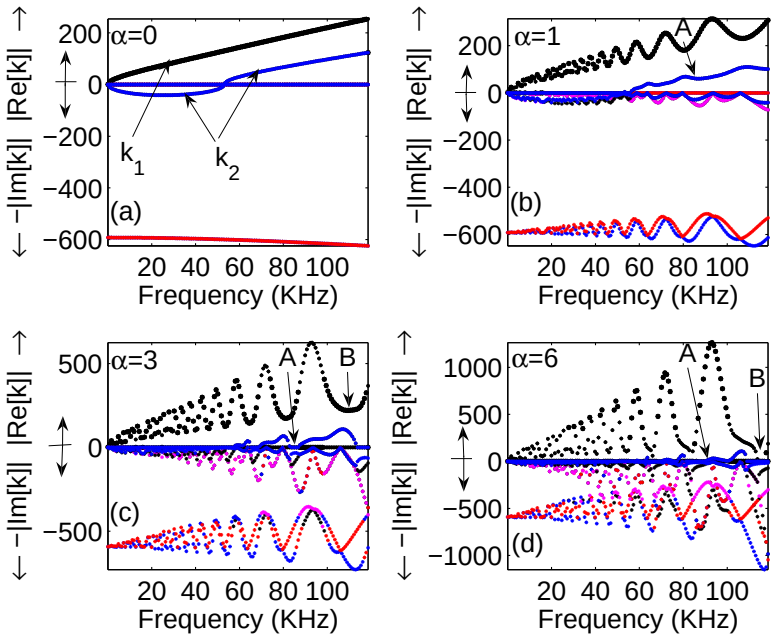

Figure 4.4: Flexural-shear wave dispersion various λ_m/λ when Q_{55} is used for evaluating the wavelength(λ) (see Eq. (4.4)), showing a tendency toward formation of stop bands for flexural and shear waves at higher frequencies (marked with arrows A and B). All sub figures are generated for $\theta = 60^o$.

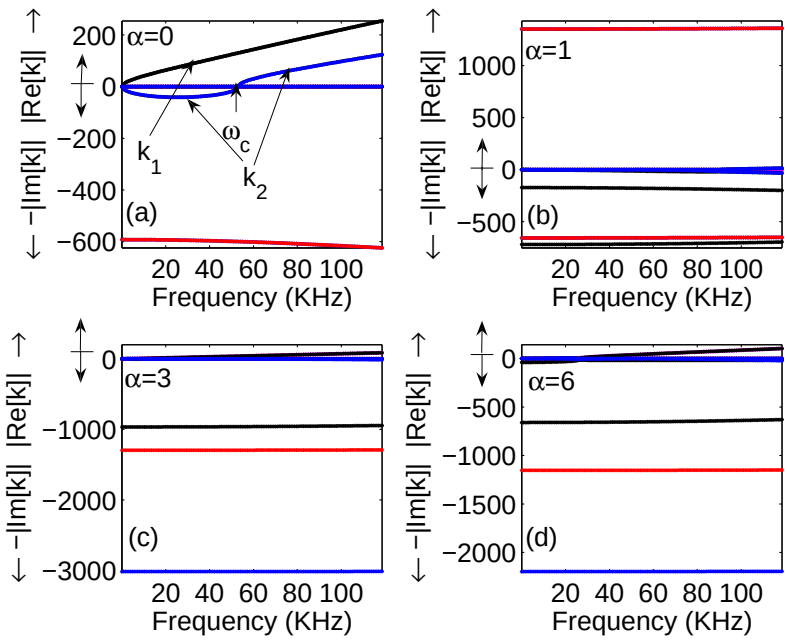

Figure 4.5: Flexural-shear wave dispersion for $\lambda = \lambda_m$ and various values of α with incident wave phase angle $\theta = 60^o$.

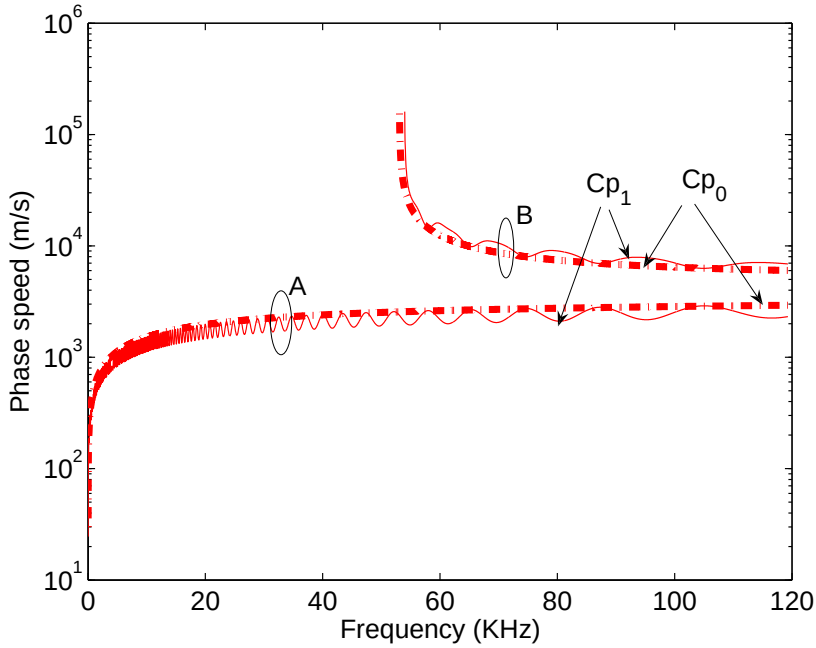

Figure 4.6: Phase speeds for $\alpha = 0$ and $\alpha = 1$. A indicates the flexural wave and B indicates the shear wave. Phase speeds for $\alpha = 0$ are indicated by Cp_0 and Phase speeds for $\alpha = 1$ are indicated by Cp_1.

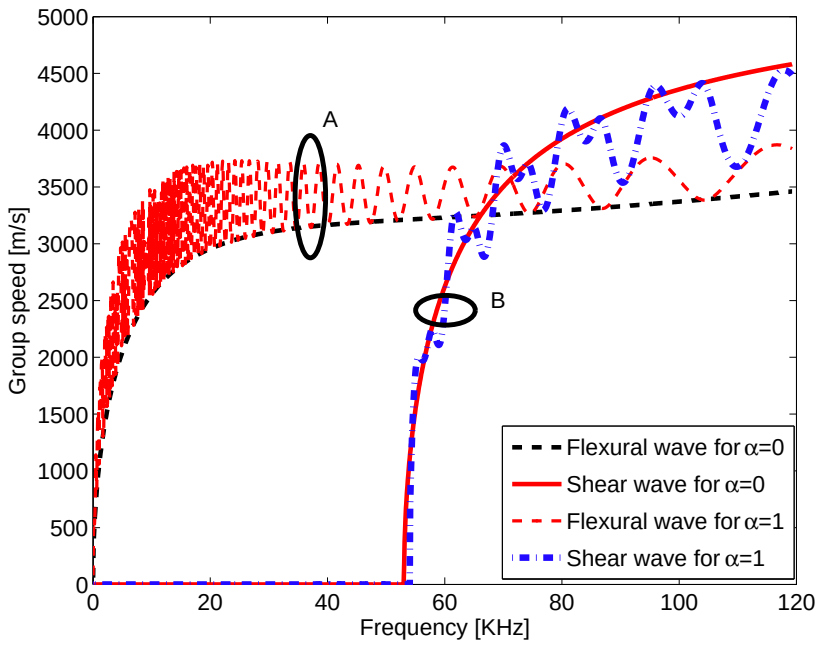

Figure 4.7: Group speeds for $\alpha = 0$ and $\alpha = 1$ are superimposed, an ellipse marked with A covering two curves indicates those two curves corresponds to flexural wave and an ellipse marked with B indicates those two curves corresponds to shear wave.

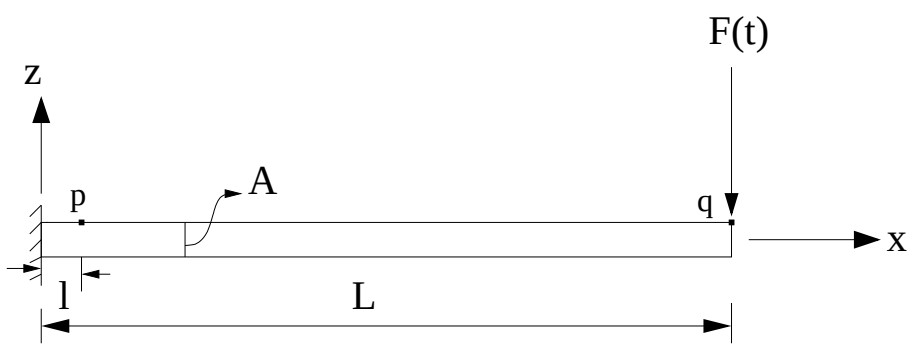

Figure 4.8: A Cantilever beam used in finite element simulation, a time dependent load P(t) is applied at tip of the beam and the velocity responce of the beam is measured at a distance of l=10 cm from the root.

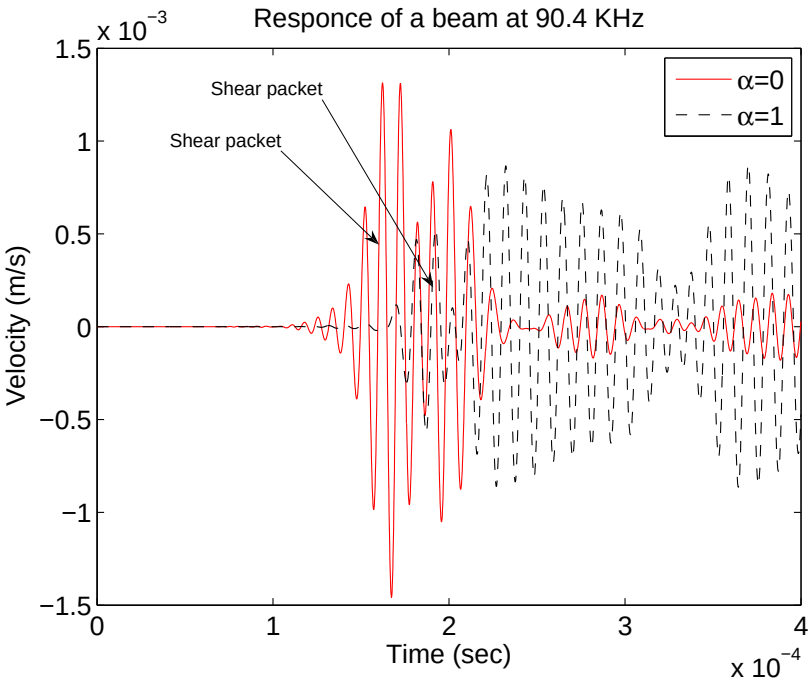

Figure 4.9: velocity history measured at a at a distance of x=10cm (Ref.Fig. 4.3) for $\alpha = 0$ and $\alpha = 1$.

Chapter 5

Static homogenization of Honeycomb panel

Static homogenization involves finding effective properties of the honeycomb panel under static loading. These are very much useful to get better understanding of wave dispersion. This static homogenization can be done by selecting a unit cell and introducing appropreate boundary conditions. The honeycomb panel is obtained by the assembly of identical cells, which are replicated in the length and width direction.

The effectie properties of the honeycomb unitcell are evaluated by using constitutive model (stress strain relations). By applying a force on the unit cell, on x-face and z-face (refer Fig. 5.1) we will evaluate deformations in x-direction and z-direction at the point of application. With the help of this deformations we can find the strains, by substituting these strains into the constitutive model one can get the effective properties of the unitcell. Therefore a costitutive model is developed for the honeycomb unitcell, this will be discussed in the next section.

5.1 Constitutive modeling

A three dimenstional honeycomb unit cell is shown in the Fig. (5.1). In the figure the unit cell is kept in dotted line box, this box represents a volume element. In the figure

L_x is the width of the cell, L_y is the depth of the unit cell and L_z is the length of the unit cell (volume element). With the help of this figure we will discuss constitutive modeling.

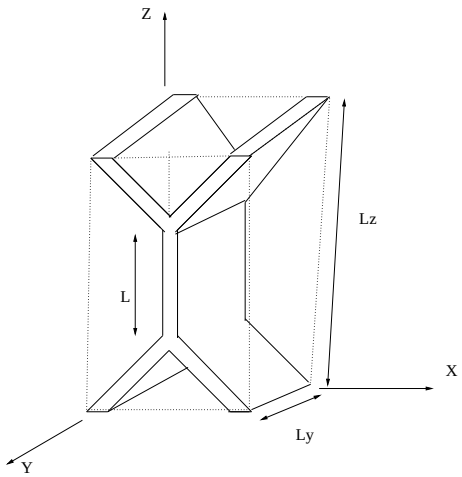

Figure 5.1: A 3-Dimensional unitcell of honeycomb panel

For evaluating effective properties of honeycomb unit cell we will consider two loading configurations one is z-loading configuration and the other x-loading configuration, these loading configurations are shown in Figs.5.3-5.4. Here z-loading configuration means the load is applied on the z-face of the unit cell and similarly x-loading configuration means load is applied on the x-face of the honeycomb unit cell as shown in Fig. 5.3 and Fig. 5.4 respectively.

For the given unit cell in the Fig. 5.1 by using two kinds of loading configurations namely $x-$ loading configuration (see Fig. 5.4) and $z-$ loading configuration (see Fig. 5.3) constitutive model is developed. In general terms constitutive modeling can be written as

$$\{\sigma\} = [C]\,\{\epsilon\}$$

The stress strain relations for $z-$ loading can be written as

$$\sigma^z_{xx} = \bar{C}_{13}\epsilon^z_{zz} + \bar{C}_{11}\epsilon^z_{xx}\ , \tag{5.1}$$

$$\sigma^z_{zz} = \bar{C}_{33}\epsilon^z_{zz} + \bar{C}_{31}\epsilon^z_{xx}\ . \tag{5.2}$$

in the above equations prefix (.) indicates the loading direction, the letter z indicates z-loading configuration. Similarly for $x-$ loading the stress strain relations can be written as

$$\sigma_{xx}^{x} = \bar{C}_{11}\epsilon_{xx}^{x} + \bar{C}_{13}\epsilon_{zz}^{x} \ , \tag{5.3}$$

$$\sigma_{zz}^{x} = \bar{C}_{31}\epsilon_{xx}^{x} + \bar{C}_{33}\epsilon_{zz}^{x} \ . \tag{5.4}$$

In $z-$ loading the stresses are calculated with reference to Fig. 5.1 and Fig. 5.3 as

$$\sigma_{zz}^{z} = \frac{2P}{L_x L_y} \ , \quad \sigma_{xx}^{z} = 0$$

because load bearing area in z direction is $L_x L_y$, similarly in $x-$ loading the stresses are calculated with reference to Fig. (5.1) and Fig. 5.3 as

$$\sigma_{zz}^{x} = 0 \ , \quad \sigma_{xx}^{x} = \frac{2P}{L_y L_z} \ .$$

Assuming the deformation in $y-$ direction is much smaller than the deformation in the $x-z$ planes (microstructure geometry) we can decouple the constitutive model. From stress strain relations Eqs.(5.1)-(5.4) one can write constitutive model as

$$\begin{Bmatrix} \frac{2P}{L_y L_z} \\ 0 \\ \frac{2P}{L_x L_y} \\ 0 \end{Bmatrix} = \begin{bmatrix} \epsilon_{xx}^{(x)} & \epsilon_{zz}^{(x)} & 0 & 0 \\ \epsilon_{xx}^{(z)} & \epsilon_{zz}^{(z)} & 0 & 0 \\ 0 & 0 & \epsilon_{zz}^{(z)} & \epsilon_{xx}^{(z)} \\ 0 & 0 & \epsilon_{zz}^{(x)} & \epsilon_{xx}^{(x)} \end{bmatrix} \begin{Bmatrix} \bar{C}_{11} \\ \bar{C}_{13} \\ \bar{C}_{33} \\ \bar{C}_{31} \end{Bmatrix} \ , \tag{5.5}$$

where

$$\epsilon_{xx} = \frac{\delta u}{L_x} \ , \quad \epsilon_{zz} = \frac{\delta w}{L_z} \ .$$

In the constitutive model Eq. (5.5) the supescript indicates loading direction, for example in ϵ_{xx}^{z} superscript z indicates z-loading condition. By using above constitutive modeling we do homogenization of the considered unitcell.

5.2 Unit load method

By the concept of 'Virtual Work' principle and and with the help of Betti's principle the unit load method is developed. According to above principles external virtual work is equal to the internal virtual work. If a truss is externally loaded, to find displacement of any joint of that truss in any particular direction, we find the member forces under the external loading and support reactions, then remove external loading and place a unit load at that joint (where we need to find displacement) in the required displacement direction. With this loading condition we evaluate member forces. Let p_i be the bar forces caused by a unit virtual load applied at the joint applied in the direction of the desired deflection and P_i the bar forces caused by the applied loading. Because bar forces p_i and P_i are constant over the whole length, the internal virtual work of a truss containing n members can be written as

$$W_i = \sum_{i=1}^{n} \frac{p_i P_i L_i}{A_i E_i}. \tag{5.6}$$

Equating the internal virtual work to external virtual work (it is found by the product of unit load and displacement (Δ) at the joint), we get in general,

$$\Delta_a = \sum_{1}^{n} \frac{\mathbf{p} P L}{AE}, \tag{5.7}$$

similarly for beams, the displacement at any joint can be evaluated as,

$$\Delta_b = \sum_{1}^{n} \int_0^{L_i} m_{x_i} \frac{M_{x_i} dx}{EI_i}, \tag{5.8}$$

where suffix a indicates displacment due to axial loading, and suffix b indicates displacement due to bending. and i=1,2,..n , indicates member (bar/beam) number, L_i is the length of the i th member and x indicates the any section with respect to a reference axis in the respective member, I_i second moment of inertia of the ith beam.

In the honeycomb unit cell the loading is in oblique direction that neither pure axial

nor pure transverse therefor we consider deflection due to both axial load and transverse loading (bending moment) on the members of the frame. Using this Unit Load method we will determine the displacements and intern effective stiffnesses of the honeycomb unitcell.

5.3 Determination of effective properties

A unitcell shown in Fig 5.3(b) is considered. By assembling this unit cell in the $X-$ derection we can get a panel with a single row as shown in Fig. 5.3(a). For the considered

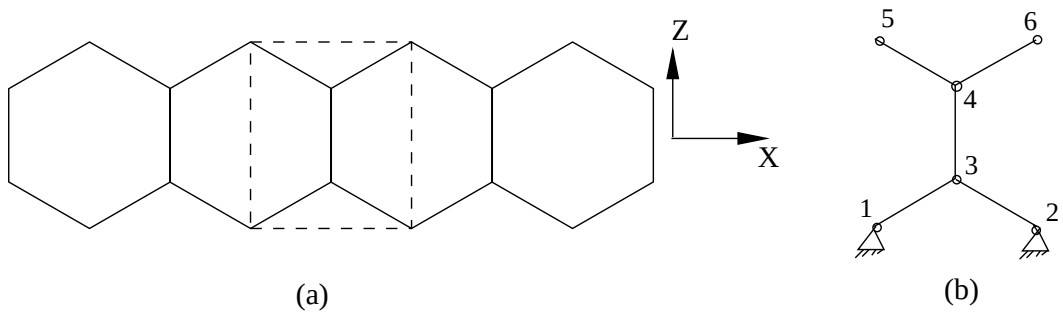

Figure 5.2: The unitcell of the honeycomb beam in the x-z plane:(a) A honeycomb panel, (b) A honeycomb unit-cell, which can produce a honeycomb panel as shown in subfigure (a) of this figure, on assembly in X-derection.

unitcell two loading conditions, z-loading and x-loading conditions are shown in the Fig. 5.3(a) and Fig. 5.4(a) respectively.

First we will consider the z-loading configuration, the free body diagram for this loading configuration is shown in Fig. 5.3(b). By using unit load method we have obtained relations for dispalcement in x-direction and z-direction at node 6 (ref. Fig. 5.3(b)), these are given below,

$$w_z = \frac{l}{AE}\left(2H_1\bar{H}_1\sin^2\theta + p\bar{H}_1\sin(2\theta) + \frac{H_1}{2}\sin(2\theta) + 2p\cos^2\theta + 2p\right)$$
$$+\frac{l^3}{3EI}\left(-p\bar{H}_1\sin(\theta) + 2H_1\bar{H}_1\cos^2\theta - \frac{H_1}{2}\sin(2\theta) + 2p\sin^2\theta\right) , \qquad (5.9)$$

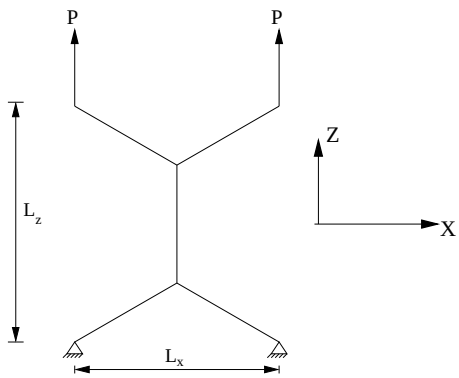

(a) Z direction loading condition for unit cell

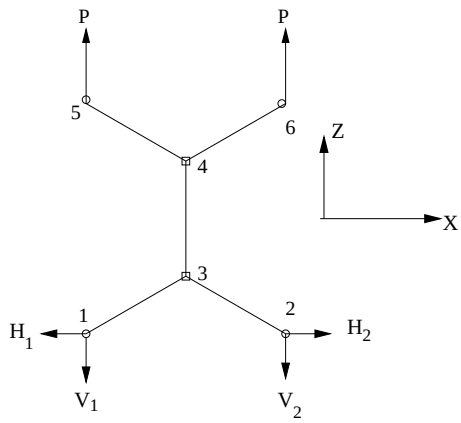

(b) Free body diagram of unitcell under Z-loading condition

Figure 5.3: honeycomb unit-cell under Z-direction loading and its free body diagram

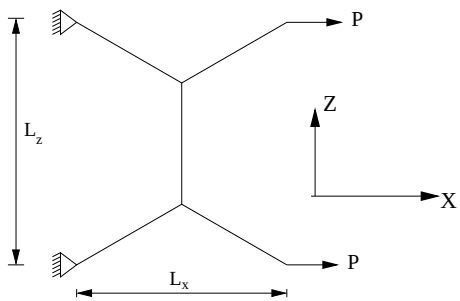

(a) X- direction loading condition for unit cell

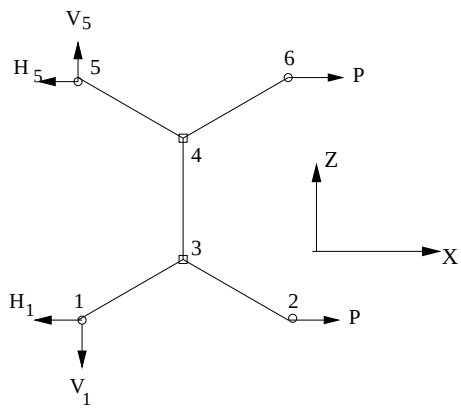

(b) Free body diagram of unitcell under x-loading condition

Figure 5.4: A honeycomb unit-cell under X-direction loading and its free body diagram

where

$$H_1 = \frac{p\sin(2\theta)\left(-\frac{1}{A}+\frac{l^2}{3I}\right)}{2\left(\frac{\sin^2\theta}{A}+\frac{l^2}{3I}\cos^2\theta\right)}$$

and

$$\bar{H}_1 = \frac{-\sin(2\theta)/(2A)+l^2/(6I)}{2\left(\sin^2\theta/A+l^2/(3I)\cos^2\theta\right)} \ .$$

$$u_z = \frac{pl}{2E}\sin(2\theta)\left(\frac{1}{A}-\frac{l^2}{3I}\right) \ . \tag{5.10}$$

Similarly for x-loading condition we have obtained displacement relations at node 6

(ref. Fig. 5.4(a)) as

$$u_x = \frac{l}{AE}\left(pv_1\sin(2\theta) + 2v_1V_1\cos^2\theta + v_1V_1 + 2p\sin^2\theta + V_1/2\sin(2\theta)\right)$$
$$+\frac{l^3}{3EI}\left(-pv_1\sin(2\theta) + 2V_1v_1\sin^2\theta + 2p\cos^2\theta - V_1/2\sin(2\theta)\right) \tag{5.11}$$

and

$$w_x = \frac{l}{AE}\left(p\bar{v}_1\sin(2\theta) + 2V_1\bar{v}_1\cos^2\theta + V_1\bar{v}_1 - V_1\cos^2\right)$$
$$+\frac{l^3}{EI}\left(-\frac{p\bar{v}_1}{3}\sin(2\theta) - V_1\bar{v}_1\frac{\sin^2\theta}{3} + V_1H_1\sin\theta\cos\theta + \frac{V_1H_1\sin\theta}{2} - \frac{V_1\sin^2\theta}{3}\right) \tag{5.12}$$

where

$$v_1 = \frac{-(1/A - l^2/(3I))\sin\theta\cos\theta}{(2\cos^2\theta + 1)/A + 5l^2/(3I)\sin^2\theta}$$

$$\bar{v}_1 = \frac{l/(AE)\cos^2\theta + l^3/(3EI)\left(H_1\sin\theta\cos\theta + \sin^2\theta + 3H_1/2\right)}{l/(AE)(1 + 2\cos^2\theta) + 5l^3/(3EI)\sin^2\theta}$$

$$V_1 = \frac{-p(1/A - l^2/(3I))\sin(2\theta)}{(2\cos^2\theta + 1)/A + 5l^2/(3I)\sin^2\theta}$$

We have also considered shear loading condition to determin C_55. The shear loading condition is shown in Fig. 5.5(a) and its freebody diagram is shown in Fig. 5.5(b). The stress strain relation is

$$\tau_{xz} = \bar{C}_{55}\gamma_{xz}\ ,$$

where $\tau_{xz} = \frac{2p}{L_xL_y}$. And strain can be calculated as

$$\gamma_{xz} = \frac{\delta u}{L_z} + \frac{\delta w}{L_x}\ ,$$

Where δu is the deflection in the x- direction and δw is the diflection in the z-direction. But for our loading configuration shown in Fig. 5.5(a) $\delta w = 0$. We will evaluate δu using unit load method. From the freebody diagram Fig. 5.5(b) one can see that, there

are 6 unknown reactions (V_1, V_2, H_1, H_2, V_5 and V_6) and we have only three equilibrium equations (Two force equilibrium equations and one moment equilibrium equation, force equlibrium equations: sum of all loads in in the x- direction is zero, sum of all loads in in the z- direction is zero, and moment about any point on the unitcell is zero.), therefore the degree of indeterminacy is 3. Therefore to evaluate these unknown reactions we are using three displacement compatibility relations in addition to equilibrium equations. The compatibility relations used are (1) total diflection at node 2 in x-direction is zero, because it is fixed joint, (2) total diflection at node 5 in the z-direction are zero and (3) total diflection at node 6 in the z-derection is zero.

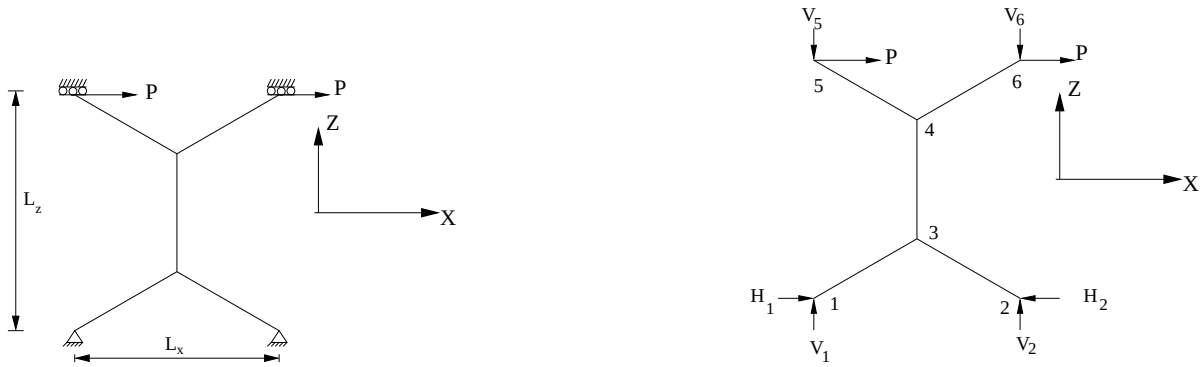

(a) Shear loading condition

(b) Freebody diagram of the unitcell under shear loading

Figure 5.5: Shear loading on honeycomb unitcell and free body diagram of unit cell under shear loading

For each compatibility relation we get an eqation, thus we get 3 equations they are given below. Compatibility equation for w_5

$$V_5\left(-\frac{1}{2}\sin(2\theta)\frac{l}{AE}+\frac{l^3}{6EI}\sin(2\theta)\right)+V_6\left(-\frac{l}{2AE}+\frac{l^3}{6EI}\right)\sin(2\theta)$$

$$+2H_2\left(\frac{l}{AE}\sin^2\theta+\frac{l^3}{3EI}\cos^2\theta\right)=-\left(\frac{2pl}{AE}\sin^2\theta+\frac{2pl^3}{3EI}\cos^2\theta\right) \tag{5.13}$$

Compatibility equation for w_6

$$V_5\left(-\frac{l}{AE}\left(1+2\cos^2\theta\right)-\frac{5V_5l^3}{3EI}\sin^2\theta\right)+V_6\left(-\frac{l}{AE}+\frac{l^3}{EI}\sin^2\theta\right)$$

$$+H_2\left(\frac{l}{AE}+\frac{l^3}{3EI}\right)H_2\sin\theta\cos\theta=-\frac{l}{AE}\left((2p\sin\theta-V_1\cos\theta)-p\sin\theta\cos\theta\right)$$
$$-\frac{l^3}{EI}\left(5p\cos\theta\sin\theta-\frac{V_1\sin^2\theta}{3}+p\sin\theta\right)\ , \tag{5.14}$$

where

$$V_1=\frac{-p(1+2\cos\theta)}{\sin\theta}$$

Compatibility equation for u_2

$$V_5\left(-\frac{l}{AE}+\frac{l^3}{EI}\sin^2\theta\right)+V_6\left(-\frac{l}{AE}(1+2\cos^2\theta)-\frac{2l^3}{3EI}\sin^2\theta-\frac{l^3}{EI}\sin^2\theta\right)$$
$$-H_2\left(\frac{l}{AE}-\frac{l^3}{3EI}\right)\sin\theta\cos\theta=-\frac{pl}{AE}\left(-\frac{1+2\cos\theta}{\sin\theta}\cos^2\theta+\sin\theta\cos\theta\right)$$
$$+\frac{pl^3}{3EI}(1+3\cos\theta)\sin\theta\ . \tag{5.15}$$

By solving above set of three equations we get support reactions V_5, V_6 and H_2.These system of equations can be solved with Matlab script. With the help of these reactions we can determine member loads and member moments. But inorder to determine diflection u_6 (ref. Fig. 5.5(b)) we need to know the member loads and moments with the unit load at node 6 in the x-direction. In the case of unit load also we get three compatibility relations in order to determine unknown support reactions. Thus by introducing these reactions into the free body diagram one can determine member loads and moments. After evaluating these member loads and moments for unit loading and as well as for external loading (2p) by substituting into Eqs.(5.7) and (5.8) one can determine diflection due to axial load and moment respectively. By doing sum of these two diflections one gets the diflection at node 6 in x-direction that is u_6. By substituting this diflection in consititutive model the evaluated value of C_{55} is 2.28×10^5.

The unit cell is perfect solid for the loading in the Y- direction, therefore the effective stiffness C_{22} is evaluated by multiplying the ratio of the projected area of the unit cell to the area of the y-face of the volume block (shown in dotted lines in Fig.5.1) to the

stiffness of the solid beam. The C_{22} is evaluated as

$$C_{22} = A_r \times E \ ,$$

where Ar is the ratio of projected area of unit cell to the area of representative volume element of unit cell. The A_r is calculed as

$$A_r = \frac{3t}{l(2\sin\theta + \sin(2\theta))} \ .$$

These results are compared with the existing results of Ashbay [2], the comparison is given in the table. 5.1. From the table one can see that, there is a difference between the present calculations (by virtual work method) and Ashbay results. This can be because of the unit cell considered is different from what Ashbay considered, they have considered a closed cell and also in the present appraoch we have considered both axial loading and bending moment in each memeber.

	C_{11}	C_{22}	C_{33}	C_{12}
New calculations	2.47×10^8	1.04×10^10	4.05×10^8	3.5×10^9
Ashbay results	3.16×10^8	1.34×10^10	3.16×10^8	1.9×10^9

Table 5.1: Comparision of effective properties evaluated from present approach with the Ashbay results (Ref.[2])

Chapter 6

Dynamic Homogenization of Honeycomb Sandwich Panel

The sandwich panel features a three dimensional frame type core with elements arranged according to a honeycomb configuration. The honeycomb configuration is laid out across the width and length of the core, as shown in Fig. 6.1. The considered sandwich panel with various loading conditions is shown in the Fig. 6.1(a). And Fig. 6.1(b) represents the core configuration of the sandwhich panel. Since the honeycomb core panel is sandwiched between two face sheets the cells are filled with air. When the panel is subjected some vibration, the air in the cells will cause pressure on the cell walls. Therefore we will consider the effect of cell wall pressure in the formulation.

The honeycomb sandwich panel, the core face sheet assembly can be decomposed into individual elements by considering the pressure acting on each element and by introducing the requisite reactions at the boundary conditions.

In the Fig. 6.1(b) one face of a honeycomb cell is marked with 'Reference face', we will consider this face and develop governing equation of motion in this plate. The reference face in local coordinate system $x\prime y\prime z\prime$ is shown in the Fig. (6.2). The loadings on the plane V_{xz} and V_{yz} are shear forces on $x\prime$ and $y\prime$ faces in the $z-$ axis direction, and moments M_{xx} and M_{yy} are moments about axes $x\prime-$ and $y\prime-$ respectively.

In order to determine the dynamic elastic properties of the honeycomb cell we use

classical plate theory, which is ideally suited for thin plates as is the case of cells with walls. The thickness of the honeycomb cell walls are very thin ($\approx$ 0.25 mm), therefore these honeycob faces can be considered as thin plates.

According to thin plate theory the displacements for flexural motion are approximated as

$$\bar{u}(x,y,z) \approx -z\frac{\partial w}{\partial x}(x,y)\ , \quad \bar{v}(x,y,z) \approx -z\frac{\partial w}{\partial y}(x,y)\ ,$$
$$\bar{w}(x,y,z) \approx w(x,y). \tag{6.1}$$

The normal and shear strains corresponding to the above deformations are

$$\bar{\epsilon}_{xx} = \frac{\partial \bar{u}}{\partial x} = -z\frac{\partial^2 w}{\partial x^2}\ ,\ \bar{\epsilon}_{yy} = \frac{\partial \bar{v}}{\partial y} = -z\frac{\partial^2 w}{\partial y^2}\ ,\bar{\gamma}_{xy} = \frac{\partial \bar{u}}{\partial x} + \frac{\partial \bar{v}}{\partial x} = -2z\frac{\partial^2 w}{\partial x \partial y}\ ,$$
$$\bar{\gamma}_{xz} = \frac{\partial \bar{u}}{\partial z} + \frac{\partial \bar{w}}{\partial x} = 0\ ,\bar{\epsilon}_{zz} = 0\ , \quad \bar{\gamma}_{yz} = \frac{\partial \bar{v}}{\partial z} + \frac{\partial \bar{w}}{\partial y} = 0\ . \tag{6.2}$$

Substituting these strains into the Hooke's law for plane stress gives

$$\bar{\sigma}_{xx} = \frac{-Ez}{1-\nu^2}\left[\frac{\partial^2 w}{\partial x^2} + \nu\frac{\partial^2 w}{\partial y^2}\right]\ , \quad \bar{\sigma}_{yy} = \frac{-Ez}{1-\nu^2}\left[\frac{\partial^2 w}{\partial y^2} + \nu\frac{\partial^2 w}{\partial x^2}\right]\ ,$$
$$\bar{\sigma}_{xy} = -2Gz\left[\frac{\partial^2 w}{\partial x \partial y}\right]\ . \tag{6.3}$$

The strain energy can be expressed as

$$U = \frac{1}{2}\int_V \left[\bar{\sigma}_{xx}\bar{\epsilon}_{xx} + \bar{\sigma}_{yy}\bar{\epsilon}_{yy} + \bar{\sigma}_{xy}\bar{\gamma}_{xy}\right] dV\ . \tag{6.4}$$

By substituting for the stresses and strains in the above strain energy equation from Eqs. (6.2)-(6.2) and integrating with respect to the thickness in the z direction leads to

$$U = \frac{1}{2}D\int\left[\left(\nabla^2 w\right)^2 + 2(1-\nu)\left[\left(\frac{\partial^2 w}{\partial x \partial y}\right)^2 - \frac{\partial^2 w}{\partial x^2}\frac{\partial^2 w}{\partial y^2}\right]\right] dxdy\ ,$$

where ∇ is the differential operator, which given as $\nabla = \frac{\partial}{\partial x} + \frac{\partial}{\partial y}$.

The kinetic energy of the plate is expressed as

$$T = \frac{1}{2}\rho h \int\int \left[\dot{w}^2\right] dxdy \ , \tag{6.5}$$

where we have made another assumption that the bending rotational inertia is negligible. The work done is expressed as

$$V = -\int\int q(x,y)wdxdy - M^b_{xx}\frac{\partial w}{\partial x} - V^b_{xz}w + M^b_{yy}\frac{\partial w}{\partial y} - V^b_{yz}sw \ , \tag{6.6}$$

where the distributed load q is due to dynamic pressure in the cell cavities and M^b, V^b are the bending moments and shear forces at the isolated cell boundaries and they are equilibriated by the forces from the neighboring cells. Using Hamilton's principle, the governing equation is obtained as

$$D\nabla^2\nabla^2 w + \rho h\frac{\partial^2 w}{\partial t^2} = q(x,y) \ . \tag{6.7}$$

By performing integration by parts we get the boundary conditions to be satisfied at any material point as

$$\begin{aligned} w \quad \text{or} \quad V_{xz} &= -D\left[\frac{\partial^3 w}{\partial x^3} + (2-\nu)\frac{\partial^3 w}{\partial x \partial y^2}\right] \ , \\ \frac{\partial w}{\partial x} \quad \text{or} \quad M_{xx} &= D\left[\frac{\partial^2 w}{\partial x^2} + \nu\frac{\partial^2 w}{\partial y^2}\right] \ , \end{aligned} \tag{6.8}$$

here D is the material constant it is defined as

$$D = \frac{Eh^3}{1-\nu^2} \ .$$

In the boundary conditions (see Eq. (6.8)) the Poisson's ratio ν enters the natural boundary conditions (bending moment and shear force) and acts to couple the variations in x to those in y. The corresponding expressions for y can be obtained by permuting x and y.

Our objective is to obtain the dynamic response of the honeycomb core under cell wall

pressure. Therefore we need to solve the governing equation of motion over the entire geometry of the sandwich panel. To obtain the dynamic response of the whole honeycomb panel first we descritize the complete honeycomb core into individual honeycomb unit cells and further each honeycomb unit cell is descritized into its individual walls. This descritization procedure is shown in the Fig. 6.3. First of all we need find the cell wall pressure q because of the air in the cell this we will be addressed in the next section.

6.1 Evaluation of pressure load on the cell walls

For a hollow honeycomb sandwich plate because of air presence there will be a coupling between the cell wall and the cavity dynamics. Therefore pressure acting on walls of honeycomb cell can be evaluated by first starting from linearized Euler equations, which are given by

$$\frac{\partial \rho}{\partial t} + \rho_0 \nabla . v = 0 \ , \tag{6.9}$$

$$\frac{\partial v}{\partial t} + \frac{1}{\rho_0} \nabla p = 0 \ , \tag{6.10}$$

where ρ_0 is air density, v is particle velocity, t is time, q is the air pressure acting the walls of the honeycomb cell and ∇ is the differential operator defined as $\nabla = \frac{\partial}{\partial x} + \frac{\partial}{\partial y}$. From gas laws change in pressure can be written as

$$dp = c^2 d\rho \ ,$$

therefore the Eq. (6.9) can be written as

$$\frac{1}{c^2}\frac{d^2 p}{dt^2} + \rho_0 \nabla . \frac{\partial v}{\partial t} = 0 \tag{6.11}$$

Eliminating $\partial v / \partial t$ from Eq. (6.10), one has

$$\frac{1}{c^2}\frac{d^2 p}{dt^2} - \nabla^2 p = 0 \ . \tag{6.12}$$

The above equation (6.12) is the governing equation for dynamic pressure on a plate. At the cell wall boundary, the linearized Euler equation (Eq. (6.10)) can be written as

$$\frac{\partial v_n}{\partial t} + \frac{1}{\rho_0}\frac{\partial p}{\partial z} = 0 \tag{6.13}$$

where v_n is the normal velocity. The normal velocity from plate can be written as

$$v_n = \dot{w} \ .$$

Using this linearized Euler equation we evaluate the pressure at the cell wall boundary. By substituting this boundary pressure in the governing equation for dynamic pressure on plate (Eq. (6.12)) we obtain the wave number in the plate due to pressure in the thickness (z) direction. Spectral form of transverse displacement and pressure are $\hat{w}(x, y, z, \omega) = \tilde{w}e^{-i(k_x(\omega)+k_y(\omega)+k_z(\omega))}$ and $\hat{p}(x, y, z, \omega) = \tilde{p}e^{-i(k_x(\omega)+k_y(\omega)+k_z(\omega))}$, therefore transverse displacement and pressure in the time dependent form, $w = \hat{w}e^{i\omega t}$, $p = \hat{p}e^{i\omega t}$. By substituting these spectral forms of transverse displacement and pressure into linearized Euler equation at wall boundary given Eq. (6.13) leads us to

$$(i\omega)^2\,\hat{w} + \frac{1}{\rho_0}(-ik_z)\hat{p} = 0 \ ,$$

$$\Rightarrow \hat{p} = \left(i\frac{\rho_0\omega^2}{k_z}\right)\hat{w} \ , \tag{6.14}$$

where k_z is the wavenumber in the fluid, this can be evaluated from governing equation for pressure in Eq. (6.12) by substituting the spectral form for pressure. That is

$$\frac{1}{c^2}(i\omega)^2 - \left[(-ik_x)^2 + (-ik_y)^2 + (-ik_z)^2\right] = 0 \tag{6.15}$$

wave numbers k_x and k_y are taken as

$$k_x = \frac{2\pi m}{L_x} \ , \quad k_y = \frac{2\pi n}{L_y} \tag{6.16}$$

by substituting for k_x and k_y in the equation (6.15) we get k_z as

$$k_z = \sqrt{\frac{\omega^2}{c^2} - \left(k_x^2 + k_y^2\right)} \tag{6.17}$$

Next we introduce this pressure q into the governing equation Eq. (6.13) and evaluate dynamic wave numbers in the plate.

6.2 Spectral Analysis

The objective is to obtain the dynamic response of the honeycomb sandwich panel. To obtain the dynamic response of the panel we need to solve the governing equation of motion over entire panel. For this we will adopt spectral finite element approach. Therefore first we need to formulate stiffness matrix for one element of the unit cell shown in Fig. 6.3. By writing the governing equation (see Eq. (6.7)) in the spectral form we can get characteristic equations, from this we can know the behavior of wave propagation, through the wave number.

The governing equation for the plate from Eq. (6.7) is

$$D\nabla^2\nabla^2 w + \rho h \frac{\partial^2 w}{\partial t^2} = q(x, y) \ ,$$

here q is the wall pressure due to air in the honeycomb cell, therefore this can be replaced with the cell wall pressure (p) from equation (6.14). Here we can also add viscous damping this gives

$$D\nabla^2\nabla^2 w + \eta h \frac{\partial w}{\partial t} \rho h \frac{\partial^2 w}{\partial t^2} = q(x, y) \ ,$$

Governing equation of plate, in the spectral form can be written as

$$\left[D\nabla^2\nabla^2 + i\eta h\omega - \rho_0 h\omega^2\right] \hat{w} = q \ , \tag{6.18}$$

by substituting the expression for dynamic pressure (q) from Eq. (6.14) we get

$$D\nabla^2\nabla^2 + i\eta h\omega - \rho_0 h\omega^2 = i\frac{\rho_0\omega^2}{k_z}$$

$$\Rightarrow \nabla^2\nabla^2 - \frac{\left(\rho h\omega^2 + \frac{i\rho_0\omega^2}{k_z} - i\eta h\omega\right)}{D} = 0 \ ,$$

this equation can be written as the product of two second order differential equations as

$$\left(\nabla^2 + \beta^2\right)\left(\nabla^2 - \beta^2\right) = 0 \ , \quad \beta^2 = \sqrt{\frac{\left(\rho h + \frac{i\rho_0}{k_z}\right)\omega^2 - i\eta h\omega}{D}}$$

these two individual differential equations each corresponds to a wave are

$$\nabla^2\hat{w}_1 + \beta^2\hat{w}_1 = 0 \ , \quad \nabla^2\hat{w}_2 + \beta^2\hat{w}_2 = 0 \ . \tag{6.19}$$

These form the basic equations for further analysis and emphasize that there are two fundamentally different modes just as there are for beams. Since the waves, possibly, can have arbitrary shapes in space, consider a representation of the form,

$$\hat{w}_1(x,y) = \frac{1}{W}\sum_m \tilde{w}_{1m}(x)e^{-i\zeta_m y} \ , \quad \hat{w}_2(x,y) = \frac{1}{W}\sum_m \tilde{w}_{2m}(x)e^{-i\zeta_m y} \ . \tag{6.20}$$

But we assume $\zeta_m = k_y$, therefore the differential equations governing the transformed displacements are

$$\frac{d^2\tilde{w}_1}{dx^2} + (\beta^2 - k_y^2)\tilde{w}_1 = 0 \ , \quad \frac{d^2\tilde{w}_2}{dx^2} + (\beta^2 - k_y^2)\tilde{w}_2 = 0 \ . \tag{6.21}$$

The coefficients of the differential equations are constant, hence the solutions are exponentials of the form e^{-ikx}. The characteristic equations associated with these solutions are

$$-k_1^2 - k_y^2 + \beta^2 = 0 \ , \quad -k_2^2 - k_y^2 - \beta^2 = 0 \ ,$$

giving the spectral relations as

$$k_1 = \pm\sqrt{\beta_n^2 - k_y^2}\ , \qquad k_2 = \pm\sqrt{\beta_n^2 + k_y^2} \tag{6.22}$$

These spectrum relations are shown in Fig. (6.4).It is noted that for any particular k_y the fist mode shows a cut-off frequency with the lower-frequency components being not propagating.

As we obtained the spectral relations (wave numbers k_1, k_2) the solution for the plate equation is

$$w(x,y,t) = \sum_n \sum_m \left[Ae^{-ik_1x} + Be^{-ik_2x} + Ce^{+ik_1x} + De^{+ik_2x}\right] e^{-ik_yx}e^{-i\omega t}\ , \tag{6.23}$$

that is, the actual solution is obtained by summing kernel solutions of the above form for many values of ω and k_y. The above solution contains a forward-moving wave A, a backward-moving wave C, and corresponding evanescent waves B and D.

We integrate this equation with respect to y, to eliminate y dependence, because we need only averaged effect in y. The integration is done along the depth of the honey comb face, between the limits of 0 to Ly.

$$w(x,y,t) = \frac{1}{L_y}\int_0^{L_y} \left(Ae^{-ik_1x} + Be^{-ik_2x} + Ce^{ik_1x} + De^{ik_2x}\right) e^{-ik_yy}e^{-i\omega t}dy\ , \tag{6.24}$$

upon integration we get

$$w(x,y,t) = i\left(Ae^{-ik_1x} + Be^{-ik_2x} + Ce^{ik_1x} + De^{ik_2x}\right) e^{-i\omega t}\gamma\ ,$$

in the spectral form we can write as

$$\hat{w}(x,y,\omega) = i\left(Ae^{-ik_1x} + Be^{-ik_2x} + Ce^{ik_1x} + De^{ik_2x}\right)\gamma\ , \tag{6.25}$$

where $\gamma = (e^{-ik_yL_y} - 1)/(L_yk_y)$.

6.3 Spectral finite element formulation

Since we have the displacement function (Eq. (6.25)) only function of x we can treat each face of the honeycomb as a panel. We consider a reference face of the honeycomb cell as shown in Fig. 6.1(b). Let us assume the two end nodes are at $x = 0$ and $x = L$ (where L=4 mm) in the local coordinate system shown in the figure. The nodal degrees of freedom are taken as w_1, θ_1 and w_2, θ_2 at the nodes 1 and 2 respectively as shown in Fig. (6.5).

Evaluating the nodal degrees of freedom from Eq: (6.25) by substituting $x = 0$ for first node and $x = L$ for second node. The nodal degrees of freedom in the spectral form are

$$\hat{w}_1 = (A + B + C + D)\gamma \ ,$$

$$\hat{\theta}_1 = (A(-ik_1) + B(-ik_2) + C(ik_1) + D(ik_2))\gamma \ ,$$

$$\hat{w}_2 = (Ae^{-ik_1L} + Be^{-ik_2L} + Ce^{ik_1L} + De^{ik_2L})\gamma \ ,$$

$$\hat{\theta}_2 = (A(-ik_1)e^{-ik_1L} + B(-ik_2)e^{-ik_2L} + C(ik_1)e^{ik_1L} + D(ik_2)e^{ik_2L})\gamma \ , \tag{6.26}$$

the nodal degrees of freedom ($\hat{w}_1$, $\hat{\theta}_1$, $\hat{w}_2$, $\hat{\theta}_2$) and constants (A, B, C, D) are indicated in the matrix form as

$$\{\hat{d}\} = \begin{Bmatrix} \hat{w}_1 \\ \hat{\theta}_1 \\ \hat{w}_2 \\ \hat{\theta}_2 \end{Bmatrix} \ , \quad \{a\} = \begin{Bmatrix} A \\ B \\ C \\ D \end{Bmatrix} \ .$$

Rewriting above nodal degrees of freedom expressions (Eq. 6.26) in the matrix form, we get

$$\begin{Bmatrix} \hat{w}_1(t) \\ \hat{\theta}_1(t) \\ \hat{w}_2(t) \\ \hat{\theta}_2(t) \end{Bmatrix} = \begin{bmatrix} 1 & 1 & 1 & 1 \\ -ik_1 & -ik_2 & ik_1 & ik_2 \\ 1e^{-ik_1L} & 1e^{-ik_2L} & 1e^{ik_1L} & 1e^{ik_2L} \\ -ik_1e^{-ik_1L} & -ik_2e^{-ik_2L} & ik_1e^{ik_1L} & ik_2e^{ik_2L} \end{bmatrix} \begin{Bmatrix} A \\ B \\ C \\ D \end{Bmatrix} \gamma \tag{6.27}$$

using matrix notations we can write in the compact form as

$$\{\hat{d}\} = [G]\{a\}\gamma \ , \tag{6.28}$$

where G represents the coefficient matrix in the Eq. (6.27). From the above equation we can find the constants matrix $\{a\}$ as

$$\{a\}\gamma = [G]^{-1}\{\hat{d}\} \ . \tag{6.29}$$

Displacement w at any point in the Eq. (6.25) can be written in the matrix notations as

$$\hat{w}(x, y, \omega) = \begin{bmatrix} e^{-ik_1x} & e^{-ik_2x} & e^{ik_1x} & e^{ik_2x} \end{bmatrix} \{a\} \gamma \ . \tag{6.30}$$

Now plugging the Eq. (6.29) into Eq. (6.30), we get

$$\hat{w}(x, y, \omega) = \begin{bmatrix} e^{-ik_1x} & e^{-ik_2x} & e^{ik_1x} & e^{ik_2x} \end{bmatrix} [G]^{-1}\{\hat{d}\} \ . \tag{6.31}$$

From the above equation we can observe that the effect of k_y is lost in the final equation but k_y has an effect indirectly in evaluating wave numbers k_1 and k_2 in Eq. (6.22).

The equation (6.31) can be expressed in the conventional notations as

$$\hat{w}(x, y, \omega) = \hat{N}_{1\times4} \left\{\hat{d}\right\}_{4\times1} \tag{6.32}$$

where N represents the nodal shape functions, these are given by,

$$\hat{N} = \begin{bmatrix} e^{-ik_1x} & e^{-ik_2x} & e^{ik_1x} & e^{ik_2x} \end{bmatrix} [G]^{-1} \ . \tag{6.33}$$

The behavior of shape functions N along the length of the plate is shown in the Fig. (6.6) at a frequency of 1591.5 rad/sec. From the figure one can observe that these dynamic shape function are satisfying essential boundary conditions at the nodal points. The shape functions $\hat{N}_1$ and $\hat{N}_3$ corresponds to transverse displacements ($\hat{w}$) at node 1 and 2

in the Fig. 6.5, the values of these shape functions are 1 at their respective nodes. And the shape functions $\hat{N}_2$ and $\hat{N}_4$ are corresponding to the slopes $\hat{\theta}_1$ and $\hat{\theta}_2$ respectively in the Fig. 6.5, therefore their derivatives are plotted in the figure, these are also having a value of 1 at their respective nodes and zero at other node.

Now we have expressed the transverse displacement function ($\hat{w}$) in-terms of nodal degrees of freedom with the help of shape functions. To get dynamic stiffness matrix we impose natural boundary conditions (shear and bending moment) at each node and in two degrees of freedom.

Assuming nodal forces and moments at each of the two nodes as F_1, M_1, F_2 and M_2. Then the equations for these nodal loads are evaluated from eq. (6.32). Since the displacement function is only function of one space dimension in x, The nodal loads can be written as

$$\hat{V}_{xz} = -D\frac{\partial^3 \hat{N}}{\partial x^3}\left\{\hat{d}\right\} \ , \tag{6.34}$$

$$\hat{M}_{xx} = D\frac{\partial^2 \hat{N}}{\partial x^2}\left\{\hat{d}\right\} \ . \tag{6.35}$$

$\hat{V}_1$, $\hat{M}_1$ is the shear force and bending moment respectively at node 1 (i.e., $x = 0$) which can be evaluated from Eq. (6.34-6.35) as

$$\hat{V}_1 = -D\begin{pmatrix} \frac{\partial^3 \hat{N}_1}{\partial x^3} & \frac{\partial^3 \hat{N}_2}{\partial x^3} & \frac{\partial^3 \hat{N}_3}{\partial x^3} & \frac{\partial^3 \hat{N}_4}{\partial x^3} \end{pmatrix}\{\hat{d}\}$$

and

$$\hat{M}_1 = D\begin{pmatrix} \frac{\partial^2 \hat{N}_1}{\partial x^2} & \frac{\partial^2 \hat{N}_2}{\partial x^2} & \frac{\partial^2 \hat{N}_3}{\partial x^2} & \frac{\partial^2 \hat{N}_4}{\partial x^2} \end{pmatrix}\{\hat{d}\} \ ,$$

similarly we can get for V_2 and M_2. Presenting these four equations in a matrix form with appropriate notations, we get,

$$\begin{Bmatrix} \hat{F}_1 \\ \hat{M}_1 \\ \hat{F}_2 \\ \hat{M}_2 \end{Bmatrix} = \begin{bmatrix} k_{11} & k_{12} & k_{13} & k_{14} \\ k_{21} & k_{22} & k_{23} & k_{24} \\ k_{31} & k_{32} & k_{33} & k_{34} \\ k_{41} & k_{42} & k_{43} & k_{44} \end{bmatrix} \begin{Bmatrix} \hat{d}_1 \\ \hat{d}_2 \\ \hat{d}_3 \\ \hat{d}_4 \end{Bmatrix} \ , \tag{6.36}$$

where $k_{11} = -D(\partial^3 \hat{N}_1/\partial x^3)$ and $k_{21} = D(\partial^2 \hat{N}_1/\partial x^2)$ similarly all other coefficients can be written. This matrix form can be written in the compact form using notations as

$$\left[\hat{K}(\omega)\right]\left\{\hat{d}(\omega)\right\} = \left\{\hat{f}(\omega)\right\} \tag{6.37}$$

Where K is the dynamic stiffness matrix and f denotes the nodal loads vector of a plate element.

6.4 Evaluation of dynamic stiffness matrix of a honeycomb unit cell

From the previous section we can evaluate the dynamic stiffness matrix of one face of the honeycomb unit cell, by using this in this section we will evaluate dynamic stiffness matrix of the honeycomb unit cell.

The schematic of the honeycomb unit cell is shown in the Fig. (6.7), it consists of 9 elements (circled numbers in the figure) and 10 nodes. The connectivity table of these elements according to global numbering is given in the following table. In the above

Table 6.1: Connectivity table for elements of honeycomb unitcell Ref.fig. 6.7

Element No.	Global nodal dof	Geometric properties	Orientation
1	2 3	A, l=L/2	$\alpha = 0$
2	3 1	A, l=L/2	$\alpha = \pi/3$
3	3 4	A, l=L	$\alpha = -\pi/3$
4	5 4	A, l=L/2	$\alpha = \pi/3$
5	4 6	A, l=L	$\alpha = 0$
6	6 7	A, l=L/2	$\alpha = -\pi/3$
7	6 8	A, l=L	$\alpha = \pi/3$
8	8 9	A, l=L/2	$\alpha = 0$
9	8 10	A, l=L/2	$\alpha = -\pi/3$

table l is the length of the element, A is cross-sectional are and α is the orientation of the element. α is calculated according to local node numbering.

After evaluating stiffness matrix for each of these element in the local coordinate system according to their geometry, we transform them into global coordinate system by using transformation matrix. Once we get the stiffness matrix for all the elements we can assemble them according to the connectivity of the elements.

The transformation matrix is evaluated using the following relation between global coordinate system and local coordinate system.

$$\begin{Bmatrix} \bar{w}_1 \\ \bar{\theta}_1 \\ \bar{w}_2 \\ \bar{\theta}_2 \end{Bmatrix} = \begin{bmatrix} \cos\alpha & 0 & 0 & 0 \\ 0 & 1 & 0 & 0 \\ 0 & 0 & \cos\alpha & 0 \\ 0 & 0 & 0 & 1 \end{bmatrix} \begin{Bmatrix} w_1 \\ \theta_1 \\ w_2 \\ \theta_2 \end{Bmatrix} . \tag{6.38}$$

Here nodal degrees of freedom with a bar on top indicates them as global representation. Hence the Transformation matrix from local coordinate system to global coordinate system can be written as

$$T = \begin{bmatrix} \cos\alpha & 0 & 0 & 0 \\ 0 & 1 & 0 & 0 \\ 0 & 0 & \cos\alpha & 0 \\ 0 & 0 & 0 & 1 \end{bmatrix} . \tag{6.39}$$

We can find the dynamic stiffness matrix of all elements of the unit cell (see Fig. (6.7)) by using the relations given in Eq. (6.36). These stiffness matrices of all the elements can be transformed to the global coordinate system (see $\bar{x}\bar{y}\bar{z}$ in the Fig. 6.7) by multiplying with transformation matrix given in Eq. (6.39). All these element stiffness matrices in the global coordinate system are assembled according to the global nodal numbering of respective element as shown in the connectivity table. 6.4.

The assembling of the individual element stiffness matrices is implemented by creating global stiffness matrix accommodating all degrees of freedom in the unit cell, this is of the order of 20×20. There are 10 nodes in the unit cell and each node has two degrees of freedom. The global stiffness matrix of the unit cell is first initialized to zero. Next the stiffness matrices of individual elements are inserted into the global stiffness matrix

according to its global node numbering. For example, element 2 has node numbers 3 and 1, the first node number 3 leads to global degrees of freedom of 5 and 6, similarly second node number 1 leads to global degrees of freedom 1 and 2. Therefore according these global degrees of freedom numbers the transformed stiffness matrix of element 2 is inserted into the global stiffness matrix. Similarly all the elements transformed stiffness matrices are assembled into the global stiffness matrix. At the common nodes there will be contribution from more than one elements so these are added together, for example at node 3 there will be contribution form elements 1,2 and 3, so all these terms are added. Thus we obtain dynamic stiffness matrix of a unit cell of honeycom panel.

6.5 Evaluation of dynamic stiffness matrix of whole honeycomb panel and model order reduction

The procedure for finding global stiffness matrix for honeycomb unit cell is described in the previous section. By using the stiffness matrix of the unit cell we can find the stiffness matrix of whole honeycomb panel shown in Fig. 6.1. For an illustration let us assume the panel is composed of nc unit cells along $z-$ axis direction and nr cells along the $x-$ axis direction in the Fig. 6.1. We have to assemble the stiffness matrices for all these cells. Since all the cells exactly resemble the unit cell we have considered the stiffness matrix for all the cells is same and this can be evaluated through the procedure explained in the last section.

From the descritization figure 6.3 we can see that for each cell assembled in the X direction there is only one common node (c_1 in the Fig. 6.3), therefore for nc cells there will be $nc - 1$ common nodes. Now we assemble this array of nc elements (in the X direction) in the Z direction to form a panel like structure. From the same figure 6.3, for each element connected in the $Z-$ direction there are two common nodes (c_2 and c_3 in the Fig 6.3). Therefore for nc cells in a row there will be $2nc$ number of common nodes. And if we assemble them in the $Z-$ direction nr such array (of nc elements) we get $2nc * (nr - 1)$ number of common nodes.

For each cell has 10 nodes for nr rows and nc columns we have a total of $10nr * nc$ nodes. Therefore the size of global stiffness matrix of whole honeycomb core is $(10nr * nc - 2nc * (nr - 1)) \times (10nr * nc - 2nc * (nr - 1))$. Thus by assembling the honeycomb unit cell in $X-$ and $Z-$ direction we get the assembled global stiffness matrix of complete honeycomb panel. Representaion of whole honeycomb panel nodal loads, stiffness matrix and nodal degrees of freedom is shown below

$$\{\bar{F}\} = [\bar{K}]\{\bar{d}\} \ , \tag{6.40}$$

here $[\bar{K}]$ represents the global stiffness matrix of complete honeycomb panel. the size of this matrix is $(10nr * nc - 2nc * (nr - 1)) \times (10nr * nc - 2nc * (nr - 1))$, where nc is the number of columns of unit cells and nr represents number of rows of unit cells to form the whole honeycomb panel. $\bar{F}$ is the global load matrix and $\bar{d}$ is the global nodal degrees of freedom matrix.

The pressure is acting on both sides for the internal elements, therefore at the internal nodes (in Fig. 6.3 indicated with i) the load is zero. Therefore we can reduce the size of the above determined global stiffness matrix into only to contain exteranal nodal degrees of freedom (inicated in the Fig. 6.3 with e). This process of reduction is called dynamic condensation.

Assuming the internal nodal degrees of freedom as slave degrees of freedom (d_s) and external nodal degrees of freedom as master degrees of freedom (d_m). Slave degrees of freedom are controlled by the master degrees of freedom therefore the name is given. Similarly nodal loads corresponding to slave degrees of freedom are represented with F_s and nodal loads corresponding to master degrees freedom are represented with F_m. With these notations Eq. (6.40) can be rewritten as

$$\begin{Bmatrix} F_m \\ F_s \end{Bmatrix} = \begin{Bmatrix} K_{mm} & K_{ms} \\ K_{sm} & K_{ss} \end{Bmatrix} \begin{Bmatrix} d_m \\ d_s \end{Bmatrix} ; . \tag{6.41}$$

Above Eq. (6.41) can be written as two individual equations, one is for master loads

(F_m) and other for slave loads (F_s), these are given below

$$F_m = K_{mm} d_m + K_{ms} d_s \ , \tag{6.42}$$

$$F_s = K_{ms} d_m + K_{ss} d_s \ . \tag{6.43}$$

But for slave degree of freedom (i.e., for internal nodes) the nodal loads are zero, therefore $F_s = 0$. The Eq. (6.43) can be written as

$$0 = K_{ms} d_m + K_{ss} d_s$$

$$\Rightarrow d_s = -K_{ss}^{-1} K_{ms} d_m$$

plugging this d_s into Eq. (6.42) will results in,

$$F_m = \left(K_{mm} - K_{ms} K_{ss}^{-1} K_{ms} \right) d_m \ .$$

Thus whole system of equations in the Eq. (6.40) is condensed to only master degrees of freedom, this is equal to the external nodal degrees of freedom (External nodal degrees of freedom are shown in the Fig. 6.3(a) with a symbol 'e'). From the Fig. 6.3(a) for each column (along Z direction) there are 4 external nodes (two on the top edge of the panel and two on the bottom edge of the plate) and for each row (along X direction) there are 2 exteranl nodes (one on the left side of the panel and the other on the right side of the panel for the configuration shown in figure 6.3)(a). Therefore there are total nuber of master degrees of freedom for a panel consisting of nc columns and nr rows of honeycomb unit cell $(4 * nc + 2 * nr) * 2$. Therefore size of the condensed dynamic stiffness matrix is $((4 * nc + 2 * nr) * 2) \times ((4 * nc + 2 * nr) * 2)$. The final condensed system of equations are represented as

$$\{F_e\} = [K_e] \{d_e\} \ . \tag{6.44}$$

Using this system of equations by applying proper boundary conditions we find dynamic response of the panel at any boundary point in the next section.

6.6 Evalution of dynamic response of the honeycomb panel

A honeycomb panel consisting of four cells in row and four cells in the column is considered shown in Fig. 6.3. From the previous section we get the condensed global system of equations of the considered honeycomb panel for master (external nodal) degrees of freedom. All these calculations finding stiffness matrix of a single plane element, assembling to get the stiffness matrix of the unit cell and further assembling to get the global stiffness matrix of whole honeycomb panel and dynamic condensation to external nodal degrees of freedom is done in the MATLAB script. Now to get the dynamic response of the panel at any nodal point on the boundary first we fix the four corners of the panel, these four corners are marked with a filled circle in the Fig. 6.3(a).

Because the four corners are fixed, the nodal degrees of freedom corresponding to those nodes are zero. We apply a point load at an external nodal point M in the Z direction in the Fig. 6.3. By solving Eq. (6.44) with these boundary conditions and applied nodal load for unknown nodal degrees of freedom (d_e) we get the dynamic response of the panel at any exteranl nodal point.

By applying a bending load of $M = 10\,Nm$ at an external node M shown in the Fig. 6.3(a) we have obtained dynamic response of the of the considered honeycomb panel at points r_1, r_2, r_3 and r_4 as indicated in the Fig. 6.3 These dynamic response of the panel with frequency is shown in the Fig.6.8.

From the Fig. 6.8 we can absorve that the dynamic response is showing some peaks at some frequencies 5 KHz 17 KHz and 55 KHz. These frequencies where the response is showing peaks are can be called resonant frequencies. Thus we the dynamic response of any size honeycomb panel is obtained by giving appropriate number of rows and columns of unitcells.

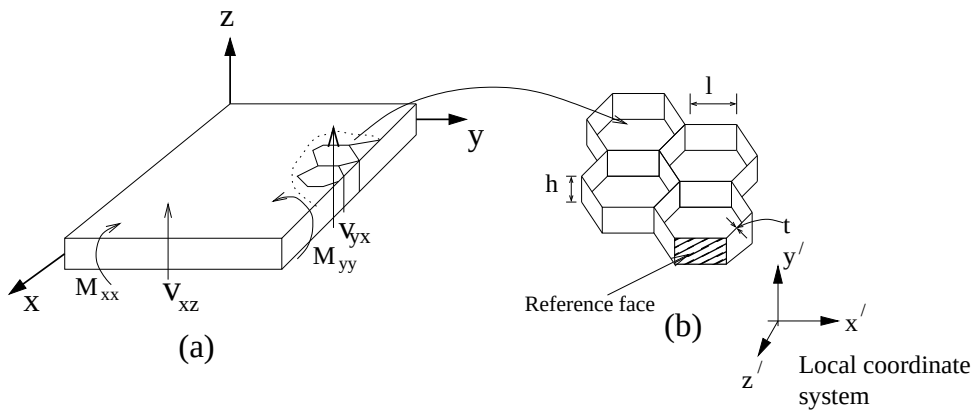

Figure 6.1: (a)Considered honeycomb sandwich panel, (b)Core configuration of the sandwich panel

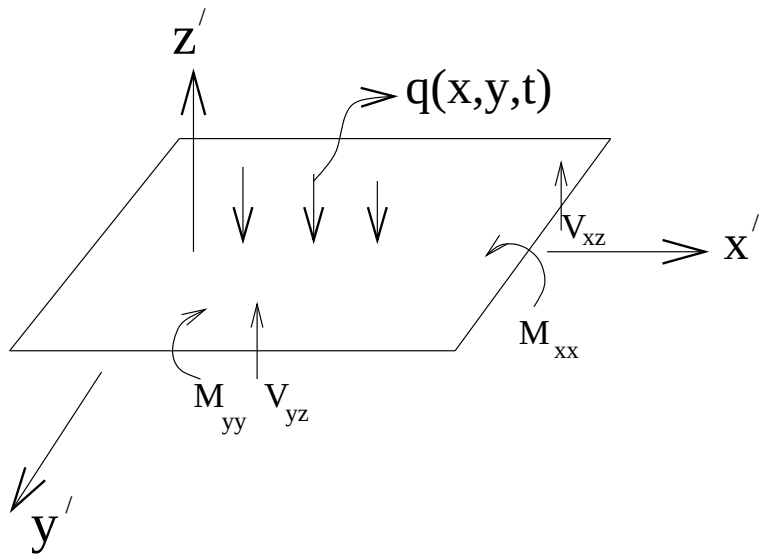

Figure 6.2: (a)Considered honeycomb sandwich panel, (b)Core configuration of the sandwich panel

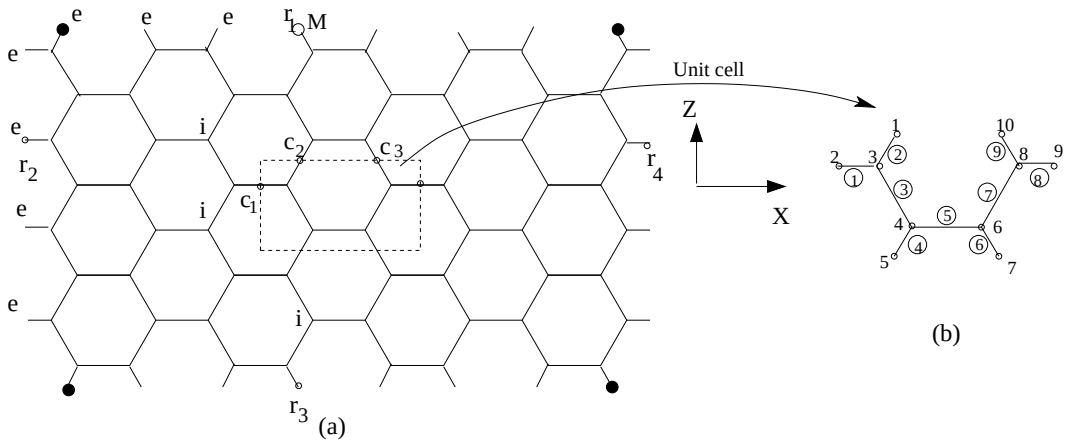

Figure 6.3: Descritization of honeycomb core configuration shown in XY plane:(a) Honeycomb core configuration, its individual unit cell is shown with dotted rectangle, (b) Unit cell further descritized into its individual plates indicated with numbers in side the circle.

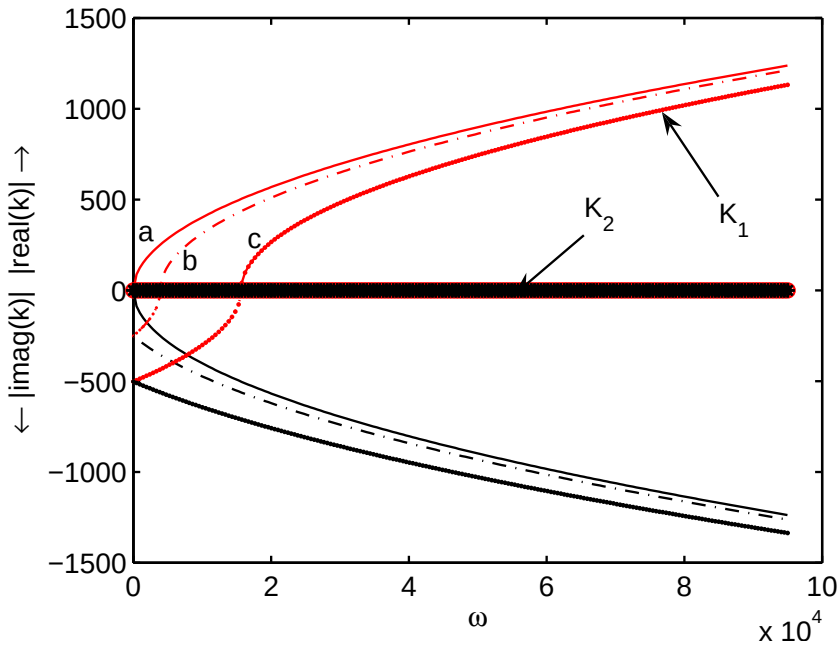

Figure 6.4: The behavior of k_1 and k_2 at different values of n in evaluating k_y, curve (a) is for $n = 0$, curve (b) for $n = 20$ and curve (c) for $n = 40$. And in all the cases $m = 0$.

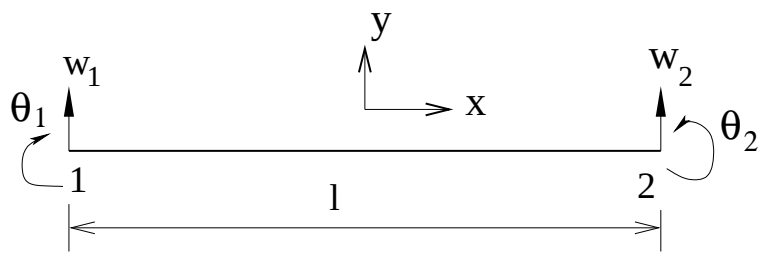

Figure 6.5: Spectral element representation of the reference face of the honeycomb cell in figure 6.1

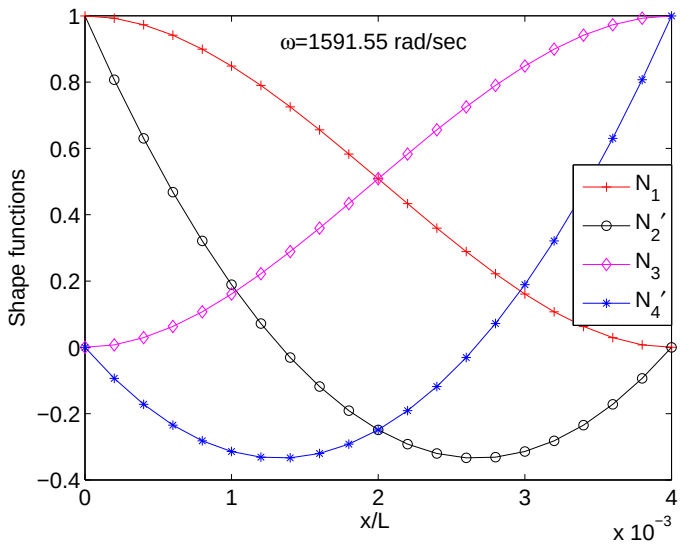

Figure 6.6: The behavior of shape functions at $10KHz$ at various x/L values

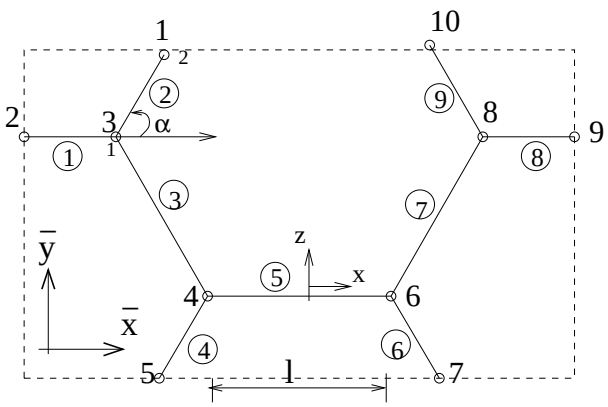

Figure 6.7: Unit cell of honeycomb panel, the circled numbers represents element numbers and remaining plain numbers represent global node numbers, small numbers 1 and 2 on the element 2 represent local node numbering.$\bar{x}$,$\bar{y}$ represents global coordinate system and x,y represents local coordinate system.

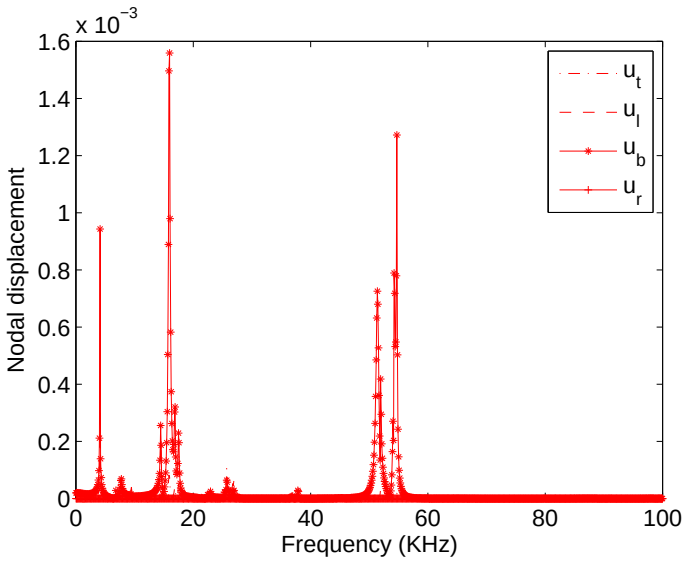

Figure 6.8: The displacement FRF at four external nodes, these are top middle, left middle, right middle and bottom middle nodes these corresponds to points r_1, r_2, r_3 and r_4 respectively in Fig. 6.3

Chapter 7

Conclusions and Future Scopes

This chapter summarizes the work done during this project and concludes with the future scope of the present work.

- The main objective of this project is to develop a modeling technique for the cellular composite beam with the modulated properties. The cellular beam is modeled by parameterization and homogenization in the wavelength scale. The modulated properties are obtained by introducing a stiffness modulation factor α. Using second order shear deformable beam theory and Hamilton's first principle, a system of wave equations are obtained and these are homogenized over the wavelength scale. The cellular laminate is assumed as being placed in two rigid baffles. With the help of the homogenized wave equations, the inplane wavedispersion and the flexural-shear coupled wave dispersion is analyzed. In the inplane wave dispersion, at higher values of stiffness modulation factor, such as $\alpha = 3$ and $\alpha = 6$, formation of repetitive stop band and pass band pattern is observed. In the flexural-shear coupled case dispersion relations are obtained for two cases, in the first case in evaluating wavelength of the incident wave on the cellular beam elastic modulus (Q_{11}) is considered, and, it has shown the shear wave is formin repetitive stop bands and pass bands, at higher vlues of α even flexural wave is showing a tendency to form stop bands. In the second case, we have considered the effect of incident shear wave, the dispersion analysis for this case shown that both flexural wave and shear

wave is forming repetitive stop bands even at lower values of stiffness modulation factor. From the group speeds and phase speeds of the modulated composite beam the tendency to form stop bands is observed. Then, the wavelength scale homogenization is verified by finite element descritization.

- Another objective is to determine the effective properties of the honeycomb panel under static loading. By selecting unitcell and with help of unit load method, and, constitutive model the effective properties of the honeycomb panel are evaluated. These effective properties are compared with existing ashbay results, new effective properties are comparable with the ashbay results.

- The final objective of the project is the, dynamic homogenization of honeycomb beam. By using spectral finite element method the dynamic response of the honeycomb sandwich panel obtained. The dynamic response of a honeycomb panel is analyzed, it is showing some resonant frequencies 7.5 KHz, 13.5 Khz and at 19 KHz.

The direct consideration of the cell wall thickness and related small scale coupling issues are an open ares of research.

Bibliography

[1] M.Ruzzene 2003. Vibration and sound radiation of sandwich beams with honeycomb truss core, *Journal of Journal of sound and Vibration*

[2] L.J. Gibson and M.F. Ashbay, Cellular Solids, Cambridge University, 1997.

[3] Suzanne L. Weekes Dispersion effects in dynamic laminates 2003 *Physica B* 338(2003), 64-66.

[4] Konstantin, A. Lurie, 1997 Effective properties of smart elastic laminatess and the screening phenomenon *International Journal of solids and structures*, Vol. 34, No.13, 1633-1643

[5] S.V. Sorokin, S.V. Grishina 2003 Analysis of wave propagation in sandwich beams with parametric stiffness modulations, *Journal of Sound and Vibration*

[6] Wang.G, Wen.X, Wen.J and Liu.Y, "Quasi-one-dimensional periodic structure with locally resonant band gap", *Journal of Applied Mechanics*, 73, 176 (2006).

[7] S.M. Ivansson, 2006. Sound absorption by viscoelastic coatings with periodically distributed cavities, *Journal of Acoustic Society of America*, 119(6), 3558.

[8] Shane C. Woody, Stuart T. Smith 2006 Damping of a thin-walled honeycomb structure using energy absorbing foam *Journal of sound and vibration* 291, 491-502

[9] J.M. Mencik and A. Berry 2006, A diffusion model for a one-dimensional structure, coupled with an auxiliary system, *Journal of Sound and Vibration*, 294, 491-502

[10] Suzzane L. Weekes 2001 Numerical computation of wave propagation in dynamic materials *Applied Numerical Mathematics* 37, 417-440.

[11] Stefano Gonella, Massimo Ruzzene, Homogenization and equivalent in-plane properties of two-dimensional periodic lattices *International Journal of Solids and Structures* 45 (2008) 2897-2915

[12] S. Balawi, J.L. Abot, A rened model for the effective in-plane elastic moduli of hexagonal honeycombs *Composite Structures* 84 (2008) 147-158

[13] Li Yongqiang, Zhu Dawei, Free flexural vibration analysis of symmetric rectangular honeycomb panels using the improved Reddys third-order plate theory *Composite Structures*